University of New Orleans

ScholarWorks@UNO

University of New Orleans Theses and Dissertations

Dissertations and Theses

5-22-2006

Investigation of Microcracking and Damage Propagation in Cross-Ply Composite Laminates

Babruvahan Hottengada
University of New Orleans

Follow this and additional works at: https://scholarworks.uno.edu/td

INVESTIGATION OF MICROCRACKING AND DAMAGE PROPAGATION IN CROSS-PLY COMPOSITE LAMINATES

A Thesis

Submitted to the Graduate Faculty of the
University of New Orleans
in partial fulfillment of the
requirements for the degree of

Master of Science
in
Engineering

by

Babruvahan Hottengada

B.E. Vishweshwariah Technological University, 2002

May 2006

Acknowledgement

With a deep sense of gratitude, I wish to express my sincere thanks to all those who encouraged and helped to complete this thesis.

First of all I would like to thank Dr. Melody A. Verges, my graduate advisor and supervisor, for giving me the oppoutunity to work on the project and for instructing me in every aspect of this project. Her knowledge and her logical way of thinking have been of great value for me and a good basis for the present thesis. Her understanding, motivation, approachableness and personal guidance have helped me develop my academic and professional career.

Secondly, I would like to thank Dr. Paul J. Schilling for giving information on the experimental procedure and analysis aspects of the thesis. His suggestions have been useful in getting end results for the thesis. I also thank him for serving in my graduate committee.

Thirdly, I would like to thank Dr. Paul D. Herrington, who kindly served on my graduate committee and supported me in this research.

I am indebted to my friends Mr. Arun Shivadas and Mr. Manesh Sankar, who spent several hours helping me generate data and perform the experiments. Finally, I would like to thank my parents, Mr. Kashi Hottengada and Ms. Kamalakshi Hottengada, and family members for their blessings and immense support; for without them, I would not be here.

Table of Contents

List of Figures

List of Tables

Abstract

The present study investigates microcracking and damage progression in IM7/977-2, IM7/5555, and IM7/5276-1 [0/90/90/0] laminates. For each material system, seven to eight small coupons were axially loaded in a tensile substage. At increments of around 50 MPa the surfaces of the specimens were inspected via optical microscopy so that a history of microcracking damage as a function of applied loading could be charted. In the IM7/977-2 laminates microcracks were found to initiate on average at around 1050MPa; microcracking initiation for the other two systems was around 850 to 900 MPa. Also, the IM7/977-2 system displayed a steeper increase in crack density as a function of applied loading than the other two systems. The IM7/5555 system was the only system that achieved a microcracking saturation density; the saturation density was found to be around 17 cracks per centimeter. While the IM7/977-2 and IM7/5276-1 systems typically broke into two pieces at failure, the IM7/5555 specimens shattered into pieces. In addition, delaminations were observed in a majority of the IM7/5555 specimens at loadings 250MPa under the failure loads.

1. Introduction

The application of composite materials can be seen from sports to bridges to satellites. Man has been using composite materials from centuries before, but in meeting the current day challenges, composite materials play a vital role in technology, making it an edge over conventional materials. The National Aerospace and Space Association (NASA) is developing a completely Reusable Launch Vehicle (RLV) in its mission of exploring outer space. This vehicle would make use of composites extensively. The composite materials in the current study finds their application extensively in major structural blocks of the aerospace structures due to having structural stability, being light-weight and being cost-effective. One concern is the use of these composites in applications such as pipelines and containment-type vessels. For these types of applications, permeability is an issue. Understanding the microcracking behavior of potential candidate composites for use in these applications is important.

The materials under investigation in this study are IM7/977-2, IM7/5555 and IM7/5276-1 carbon fiber epoxy resin matrix advanced composite materials in the [0/90/90/0] orientation. These composite materials were supplied by Lockheed Martin Corporation to investigate the microcracking behavior of these material systems. Preliminary studies for these systems included loading each specimen to some predetermined load and then inspecting it via X-ray microtomography [1]. The microcracking density obtained from this inspection then allowed for one point from each sample to be plotted on a microcracking density versus applied stress plot. While this method allowed for a better assessment of three-dimensional damage that had formed in the specimen, a history of damage for each specimen could not be charted.

In this study, the primary aim is to obtain microcracking progression data as a function of loading for each specimen. Optical Microscopy (OM) is used to scan the external surface of the laminate in real time while the composite coupon is subjected to a tensile load. This allows the number of microcracks formed across the thickness of the ply to be counted. A secondary aim is to obtain damage progression data (mainly due to delamination) that evolves in the specimens at higher loads. A final aim of the study deals with predicting the microcracking fracture toughness of the material systems based on the data obtained in these studies.

The following chapter reviews current literature related to damage in composites, microcracking initiation and propagation, and the finite fracture approach for predicting matrix microcracking. Chapter 3 presents a discussion of the experimental set-up and procedures. Results of the experimental data, including a comparison of microcracking progression in the three material systems, a comparison of damage progression in the three systems, as well as the calculation of the microcracking fracture toughness of the IM7/977-2 system, are presented in Chapter 4. Conclusions and recommendations for future work are discussed in Chapter 5.

2. Literature Review

A composite material is a combination of two or more materials on a macroscopic scale to form a useful third material. From the matrix point of view composites can be divided into three main categories: polymer matrix, metal matrix and ceramic matrix composites. Most composites used in the industry, as well as in the present study, are polymer matrix composites. From the reinforcement point of view there are two common types: fiber-reinforced and particle-reinforced composites. Fiber-reinforced composites have many variations like single-layer composites, multi-layer composites, continuous-fiber-reinforces composites, discontinuous-fiber-reinforced composites, unidirectional-reinforced composites, bidirectional-reinforced composites, laminates and hybrids [2]. Particle-reinforced and discontinuous-fiber-reinforced composites are also classified as random orientation and preferred orientation according to the orientation of reinforcement in the matrix. The composite of the present study is classified under fiber-reinforced-multi-layer-laminate (angle-ply).

Compared to conventional metallic materials, composites have a very high stiffness, good corrosion resistance and fatigue properties, better dimensional stability over a range of temperature, and better impact resistance and tolerance [2]. As a result of their superior properties, composites have brought a substantial impact on aerospace, sports and automotive industries.

Carbon fibers are predominantly high-strength and high-modulus, reinforcements used in the fabrication of high-performance resin-matrix composites. The current technology of producing

carbon fibers generally centers on the thermal decomposition of various organic precursors. However, currently available carbon fibers are made using one of the three precursor materials: pitch, rayon fibers or polyacrylonitrile (PAN). These materials typically have tensile strengths of 1550 MPa (Pitch), 2070-2760 MPa (Rayon) and 2480-3100MPa (PAN). Fiber diameters vary from 6.5-10um [2].

Epoxy resin is classified as polymer-thermosetting matrix. Thermosetting matrix materials have cross-linked or network structures with covalent bonds between all molecules. They do not soften but decompose on heating. Once solidified by the cross- linking (curing) process they can not be reshaped. Most properties like strength, stiffness, thermal expansion, conductivity and permeability are highly dependent on variables like temperature, environment and strain rate [2]. The materials used in the current study are IM7/977-2, IM7/5555 and IM7/5276-1. IM7 is the type of carbon fiber and 977-2, 5555 and 5276-1 are the matrix systems.

2.1 Microcracking in Composite Materials

Composite materials can experience several different forms of damage including: matrix microcracking, fiber pull-out, fiber-matrix debonding, and fiber breakage etc. Since the focus of the current study is on the development and progression of microcracking in cross-ply laminates, the next few sections are dedicated to (1) discussing microcracking trends in laminates and (2) presenting the finite fracture approach for predicting microcrack initiation and progression in composites.

The first form of damage in laminates is usually matrix microcracking. Matrix microcracking is an intralaminar, a.k.a. ply, crack that traverses the thickness of the ply and runs parallel to the fibers in the ply. The most common observation of microcracking is cracking of 90° plies during axial loading in 0° direction. These microcracks are transverse to the loading direction and, are thus, sometimes called transverse cracks. The term matrix microcracks, microcracks, intralaminar cracks, ply cracks, and transverse cracks are used interchangeably in the composite literature.

Microcracks can be found during tensile loading, during fatigue loading, during changes in temperature and during thermo-cycling. Microcracking can form in any ply, but forms predominantly in the plies that are off-axis to the loading direction. The immediate effect of microcracking is to cause degradation in the thermomechanical properties of the laminate including change in all effective moduli, Poisson's ratios, and thermal expansion coefficients. If a given design can not tolerate microcracking-induced degradation in properties, then the formation of microcracking constitutes failure of the design. A secondary effect of microcracking is that they nucleate other forms of damage. For example, microcracking can induce free edge delaminations, matrix-crack-tip induced delaminations, creep, resin embitterment, fiber-matrix debonding, oxidation of matrix material, fiber breaks, or provide pathways for entry of corrosive liquids. Such damage modes may subsequently lead to laminate failure [4]. The process by which microcracking forms, the effects they have non laminate properties, and their role in nucleating new forms of damage are all important problems in the analysis of failure of composite laminates.

2.2 Microcracking Initiation

Microcracking is the first form of damage occurring in laminates having 90° plies. The formation of the first crack is the initiation of the microcrack. It has been demonstrated by other researchers that there is a significant effect of 90° ply thickness on the strain to initiate microcracking. As the thickness of 90° plies becomes smaller than the thickness of the 0° plies, the strain to microcracking initiation increases. When the microcrack intitiates it propagates across the entire cross-section of the 90° plies in the experimental tie scale. As the thickness of the 90° plies becomes very small, the microcracks are suppressed entirely and the laminates fail before the initiation of microcracking. The first-ply failure theory assumes that the first ply cracks or fails when the strain in those plies reaches the strain to failure those plies [5, 6]. It furthermore assumes that the ply failure can be determined from experiments on isolated unidirectional laminates. Thus, the first-ply failure theory predicts that the strain to initiate microcracking will be independent of ply thickness; this prediction contradicts all the experimental observations of microcracking. Thus, the optimum design on experimental results is to make 90° plies as thin as possible.

Besides $[0_n/90_m]_s$ laminates, microcracking may initiate in the 90° plies of any laminates. Studies show microcracking occurrence in $[\pm30/90_n]_s$ and $[\pm60/90_n]_s$. There has been also work on $[90_n/0_m]_s$ laminates and other cross-ply laminates with the 90° plies on the outer plies [7,8,9]. The universal observation is that the microcracking behavior of $[90_n/S]_s$ laminates differ from the those of the corresponding $[S/90_m]_s$ laminates. In particular, the strain to initiate microcracking is lower for laminates with the outer 90° plies than for the laminates with the central 90° plies. The results from $[S/90]_s$ laminates show that the supporting plies constrain the 90° plies and can inhibit microcracking. Surface 90° plies however are only constrained on one side and thus

microcracking initiates easier. Other statistical arguments are that as the thickness of the 90° plies decrease; the smaller the volume of ply material will have statistically fewer flaws and naturally show higher strain to failure.

2.3 Microcrack Progression

Additional loading of a specimen containing a microcrack will result in the formation of additional microcracking. Several experiments have described the features of multiple microcracks [10]. For all laminates there is no microcracking until some onset stress that corresponds to the initiation of microcracking. After the initial microcrack, the microcrack density typically increases very rapidly. At high crack density, the microcracking slows down and approaches a saturation damage state. The initial rapid raise varies between different materials types with some laminates having a slower increase in crack density or a more sigmoid shape than other laminates. The rate of initial raise has been associated with manufacturing defects or statistical inhomogeneities in the ply materials [11].

Other observations are that the onset stress decreases as the thickness of the 90° plies increases. On continued loading however, the situation reverses- thinner 90° ply groups eventually develop more microcracks than thicker 90° ply groups. In other words, the saturation crack density is inversely related to the thickness of the 90° plies.

For $[90_m/0_n]_s$ laminates the characteristic curves are the same as for $[0_n/90_m]_s$ laminates; i.e., after the onset of microcracking there is rapid raise in microcrack density followed by a slowing towards microcracking saturation at high applied loads. Comparing the results for $[0_n/90_m]_s$ and

$[90_m/0_n]_s$ laminates shows that microcracking starts at lower loads in $[90_m/0_n]_s$ laminates than in $[0_n/90_m]_s$ laminates. However, $[0_n/90_m]_s$ laminates eventually develop more microcracks at saturation [9]. Another difference between $[0_n/90_m]_s$ and $[90_m/0_n]_s$ laminates is the final characteristic damage state. $[0_n/90_m]_s$ laminates develop roughly periodic array of microcracks, while $[90_m/0_n]_s$ develop an anti- symmetric array of microcracks. The curved microcracks in $[0_n/90_m]_s$ due the interactions between microcracks at high crack densities causes the maximum principal stress to shift to a location near the 0/90 interface and close to an existing crack [12].

2.4 Finite Fracture Mechanics Approach for Predicting Microcracking

The finite fracture mechanics model has been developed by applying a suitable modification to the conventional fracture mechanics approach. Conventional fracture mechanics deals with crack propagations; however microcracking of laminates is an instantaneous occurrence of fracture events in an experimental time scale and involves formations of finite amount. Besides microcracking, various other forms of damages such as fiber breaks, interfacial debonds, delamination and etc are also fracture events restricts the use of conventional fracture for analysis. The aim of the finite fracture mechanics models is to predict the effective thermomechanical properties of the laminates with the given amount of microcracking and to predict the conditions which lead to the formation of microcracking. Most of the studies have focused on the microcracking of 90° plies in which the laminates are predominately loaded with tensile loads perpendicular to the fiber in those plies. There are several reasons for this approach. In such laminates, the microcracks that form in the 90° plies typically span the entire cross-section of the 90° plies. Thus, the potentially three-dimensional problem can be reduced to

two dimensions by viewing the edges of the laminate and assuming that the crack propagates through the entire width.

Finite fracture mechanics is an energy model of fracture mechanics to predict when microcracking will occur [9]. Using this approach, the next microcrack is predicted to form when the total energy released by the formation of that microcrack reaches the critical energy release rate for microcracking. This material property, denoted by G_{mc}, is called the microcracking fracture toughness. The microcracking fracture toughness is a material property; i.e., it is independent of ply lay-up. This model requires stress analysis to calculate the total energy released by the formation of the next complete microcrack; this term can be denoted as G_m. Once this energy release rate is known, finite fracture mechanics can be used to predict the conditions required to form microcracks or to predict the experimental results for crack density as a function of applied loads.

Following the work by Liu and Nairn [11], the energy release rate, G_m, can be expressed as

$$G_m = \left(\frac{E_T}{E_C} \sigma_o - \frac{\Delta \alpha T}{C_1} \right)^2 C_3 t_1 Y(D) \qquad (1)$$

where E_T and E_C are the axial moduli of the ply material and the x-direction modulus of the cross-ply laminate, σ_o is the tensile stress in the x-direction, $\Delta \alpha$ is the difference between the transverse and longitudinal thermal expansion coefficient, C_1 and C_3 are constants which are function of other material properties like G_A, G_T, v_A, v_T (axial and transverse shear moduli and Poisson's ratio, respectively) and t_1 is the thickness of the 90° ply . The energy release rate scaling factor, $Y(D)$, can be expressed as

$$Y(D) = LW \frac{d}{dA} \frac{\sum_{i=1}^{N} \chi(\rho_i)}{\sum_{i=1}^{N} \rho_i} \qquad (2)$$

where ρ is defined as a/t_1, $2a$ is the distance between the existing cracks, L is the specimen length, W is the width, and A is the cross-sectional area of the specimen. $\chi(\rho)$ in this equation is given by

$$\chi(\rho) = 2\alpha\beta(\alpha^2 + \beta^2) \frac{\cosh 2\alpha\rho - \cos 2\beta\rho}{\beta \sinh 2\alpha\rho + \alpha \sin 2\beta\rho} \qquad (3)$$

where α and β are constants dependent on the same material properties as C_1 and C_3 are.

Considering a sample with N microcracks, the crack spacing between each crack is characterized as ρ_1, ρ_2, ρ_3, ρ_4, ... ρ_N. Here, $<\chi(\rho)>$ is expressed as

$$< \chi(\rho) >= \frac{1}{N} \sum_{i=1}^{N} \chi(\rho_i) \qquad (4)$$

Crack density is given by $D = N/L$. After the formation of the new crack at the k_{th} interval at $\xi = 2\delta-\rho_k$, with ξ defined as x/t_1, $<\chi(\rho)>$ is expressed as

$$< \chi(\rho) >= \frac{1}{N+1} \left[\left(\sum_{i=1}^{N} \chi(\rho_i) \right) - \chi(\rho_k) + \chi(\rho_k - \delta) + \chi(\delta) \right] \qquad (5)$$

It is expected by the researchers that cross-ply laminates tend to form regularly spaced microcracks; during a typical experiment observation it is not known where the next new crack will form. Assuming the next new microcrack forms in the crack interval whose spacing is equal to the average crack spacing, ρ_k can be expressed as $\rho_k = 1/(2t_1D)$. Also assuming the new crack forms at the mid-span of the existing crack interval, δ can be expressed as $\delta=\rho/2$. With these assumptions the function $Y(D)$ simplifies to

$$Y(D) = 2\chi(\rho/2) - \chi(\rho) = 2\chi\left(\frac{1}{4t_1 D}\right) - \chi\left(\frac{1}{4t_1 D}\right) \tag{6}$$

The above equation is agreeable for the assumptions made earlier and in real experimental observations where the crack density (D) is in the low crack density regime. In this low crack density area the energy release by the formation of new crack formed between the two existing cracks is independent of crack spacing. However, when the crack density gets higher and there is a distribution of crack spacing, energy released by the formation of the new microcrack in a small crack interval will be lower than the energy released by the formation of new microcrack in a large crack interval. To compensate for this effect, Nairn and Liu [11] introduced a new parameter f and modified equation (6) to include this f parameter as follows:

$$Y(D) = 2\chi(f\rho/2) - \chi(f\rho) = 2\chi\left(\frac{f}{4t_1 D}\right) - \chi\left(\frac{f}{4t_1 D}\right) \tag{7}$$

where the average f is the average ratio of the size of the crack interval in which the crack forms to the average crack spacing. Typical f values vary in the range of 1.0 to 1.44 [11].

3. Experimental Procedure

There were three composites investigated in the current study: IM7/977-2, IM7/5555 and IM7/5276-1. All the specimens were cross-ply laminates of the [0/90/90/0] lay-up. From each composite panel six specimens were tested until failure and two specimens were tested up to a pre-determined load preceding failure. The first aim of the experimental testing is to generate microcracking density data for each composite. As noted by Nairn [11], microcracking density (here, noted in number of microcracks per centimeter) as a function of applied loading is necessary in determining the microcracking fracture toughness of the composite. This requires loading each coupon to pre-determined stresses (whether it is the failure load or some high load preceding failure) at pre-determined stress intervals. A second objective is to analyze the microcracking progression in each of the three different composites. For each specimen examined for this analysis, the procedure entailed finding the distance between each crack across the entire viewing span at each pre-determined stress level. Recall that in using the finite fracture mechanics approach for predicting microcrack progression, it is assumed that additional cracks always initiate at the center of the previous crack spacing. However, in practical applications this is not always the case. The current analysis is being performed to study the experimental behavior in hopes of determining an f parameter (introduced by Nairn [11]) for each of the composites under investigation. The third objective of these studies is to analyze the damage progression in each of the specimens to better understand the failure characteristics of each of these composites.

3.1 Specimen Information

IM7/977-2, IM7/5555, and IM7/5276-1 composite panels, measuring 12 inches by 12 inches, were manufactured by a vacuum bagging procedure at Lockheed Martin Space System Company-Michoud Operations. Ultrasonic testing was performed prior to cutting these panels. No initial damage was identified. The total thickness of the panels varied with IM7/977-2 being 0.55mm, IM7/5555 being 0.55mm and IM7/5276-1 being 0.60mm.

3.2 Specimen Preparation

Each panel was numbered and cut into four quadrants; each quadrant was numbered in a clockwise fashion beginning with the top right quadrant. This quadrant piece was cut further into four pieces and numbered in the same manner as before. These smaller pieces were then cut into specimens measuring 60mm x 5mm. A typical numbering will look like 5-I-IV-3. Here the number 5 designates the IM7/5555 composite. I-IV-3 denotes the location that the specimen was cut from the panel. This specimen was the third one cut from the 3in by 3in quadrant IV section of the 6in by 6in quadrant I section. The panels are cut in such a manner that the final specimen is cut along 0° plies and 0° plies are on the outer surface. The above dimensions are required for the sample to accommodate both the tensile substage and the X-ray microtomography machine. All cutting is performed with a circular diamond cutter at suitable speed with continuous flow of lubricant ensuring proper dimensions and heat removal. The blade of the cutter is a diamond metal bonded, wafer blade. Tables 3.1, Table 3.2 and Table 3.3 display the final dimensions and variation in these dimensions across the length of each specimen tested.

Table 3.1 Specimen Widths and Variations for Material System IM7/977-2.

Specimen	Width (mm)	Width (mm)	Difference (mm)	Final Width (mm)
2-I-II-5	4.79	4.77	0.02	4.78
2-I-II-6	4.84	4.86	0.02	4.85
2-I-II-7	5.14	5.22	0.08	5.18
2-I-III-1	4.57	4.56	0.01	4.565
2-I-III-3	5.02	5.03	0.01	5.025
2-I-III-9	4.87	4.81	0.06	4.84
2-I-III-4	4.80	4.82	0.02	4.81
2-I-III-5	4.88	4.90	0.02	4.89

Table 3.2 Specimen Widths and Variations for Material System IM7/5555.

Specimen	Width (mm)	Width (mm)	Difference (mm)	Final Width (mm)
5-I-II-1	4.57	4.55	0.02	4.56
5-I-II-2	4.84	4.82	0.02	4.83
5-I-II-3	4.88	4.92	0.04	4.90
5-I-II-5	4.95	4.97	0.02	4.96
5-I-IV-1	4.54	4.54	0.00	4.54
5-I-IV-3	4.77	4.64	0.13	4.76
5-I-IV-8	4.41	4.44	0.03	4.425
5-I-I-3	4.96	4.95	0.01	4.955

Table 3.3 Specimen Widths and Variations for Material System IM7/5276-1.

Specimen	Width (mm)	Width (mm)	Difference (mm)	Final Width (mm)
6-II-IV-1	5.04	5.08	0.04	5.06
6-II-IV-2	4.75	4.78	0.03	4.765
6-II-IV-4	5.01	5.10	0.09	5.055
6-II-IV-5	4.78	4.75	0.03	4.765
6-II-IV-6	5.47	5.46	0.01	5..465
6-II-IV-7	4.98	5.01	0.03	4.995
6-II-IV-3	4.87	4.86	0.01	4.865

To obtain a good quality surface for optical microscopy observation while testing the cut specimens were polished on the cross-section surfaces using P-2400 grit silicon carbide polishing paper on a rotating polishing machine. The specimen surface was to be held parallel to the polish paper to ensure regular surface. Water was fed continuously over the polish paper to remove dirt and water. The speed of polishing machine was optimized so as to avoid the splitting of plies and the polishing paper was changed periodically.

To prevent the specimen from slipping and crushing under the clamps of the tensile substage, aluminum tabs were glued on the either ends of the specimen. Due to tightening of the jaws of the tensile substage there is a stress concentration at the grips of the jaws and the tabs provide a smooth gripping surface and distribute stress and prevent specimen from further crushing. These aluminum tabs are made of aluminum sheet of 20 gauge (0.80 mm) cut into approximately

10mm x 20mm pieces. The specimen was glued using Loctite E-120HP Hysol epoxy adhesive. Before gluing the specimen the surfaces of the specimen and the aluminum tabs were made rough using 2-100 medium sand paper to ensure perfect bonding. The glue was mixed using a static mixer. An optimal quantity was used so that the glue itself does not fail under shear load. The glued specimen was cured at room temperature eight to ten hours before testing. Figure 3.1 shows four specimens after preparation.
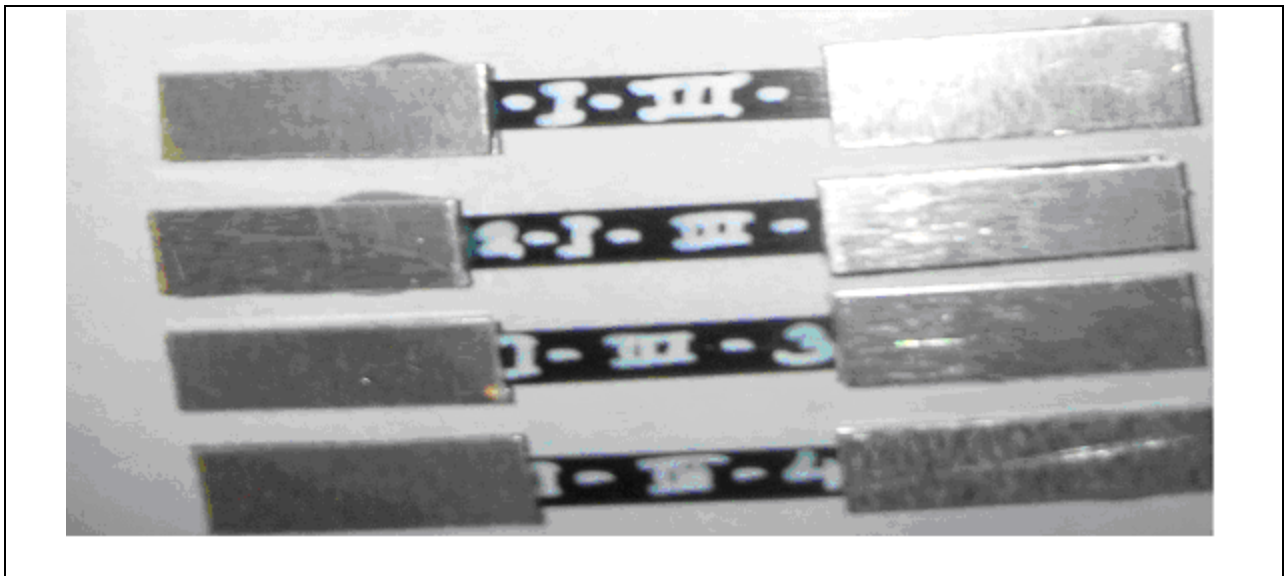

Figure 3.1 Specimens after Preparation

3.3 Experimental Set-up

Tensile testing was done using 2000 lb capacity tensile substage. The test setup comprises of a tensile substage, data acquisition system and mechanical testing software MTestWindows supplied by ADMET, Inc. Figure 3.2 depicts the experimental setup. Figure 3.3 shows a close-up view of a specimen in the substage.

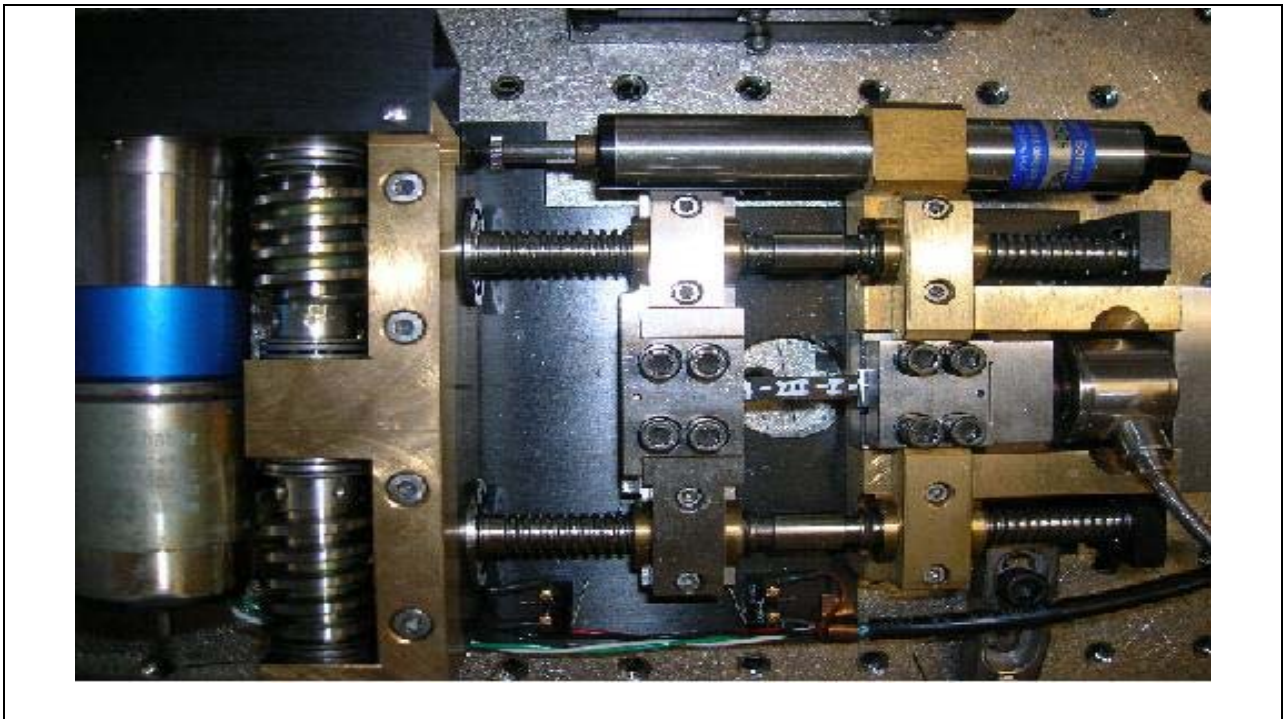*Figure 3.2 Experimental Setup.*

Figure 3.3 Close-up view of a Specimen in the Substage.

Figure 3.4 depicts a typical screen of the software. This window displays five smaller windows on the screen; beginning from the top left in a clockwise order they are: the load on the specimen, the stress, the displacement of the cross-heads, the strain and a load versus time graph. All windows display the live values, peak values, and rate of change in the parameter values at all times. Usually all the windows begin at zero except the displacement windows with some oscillating values at a third decimal place. Before beginning the test always it was noted to minimize the oscillation by clicking the zero button on the right hand side of the displacement window.
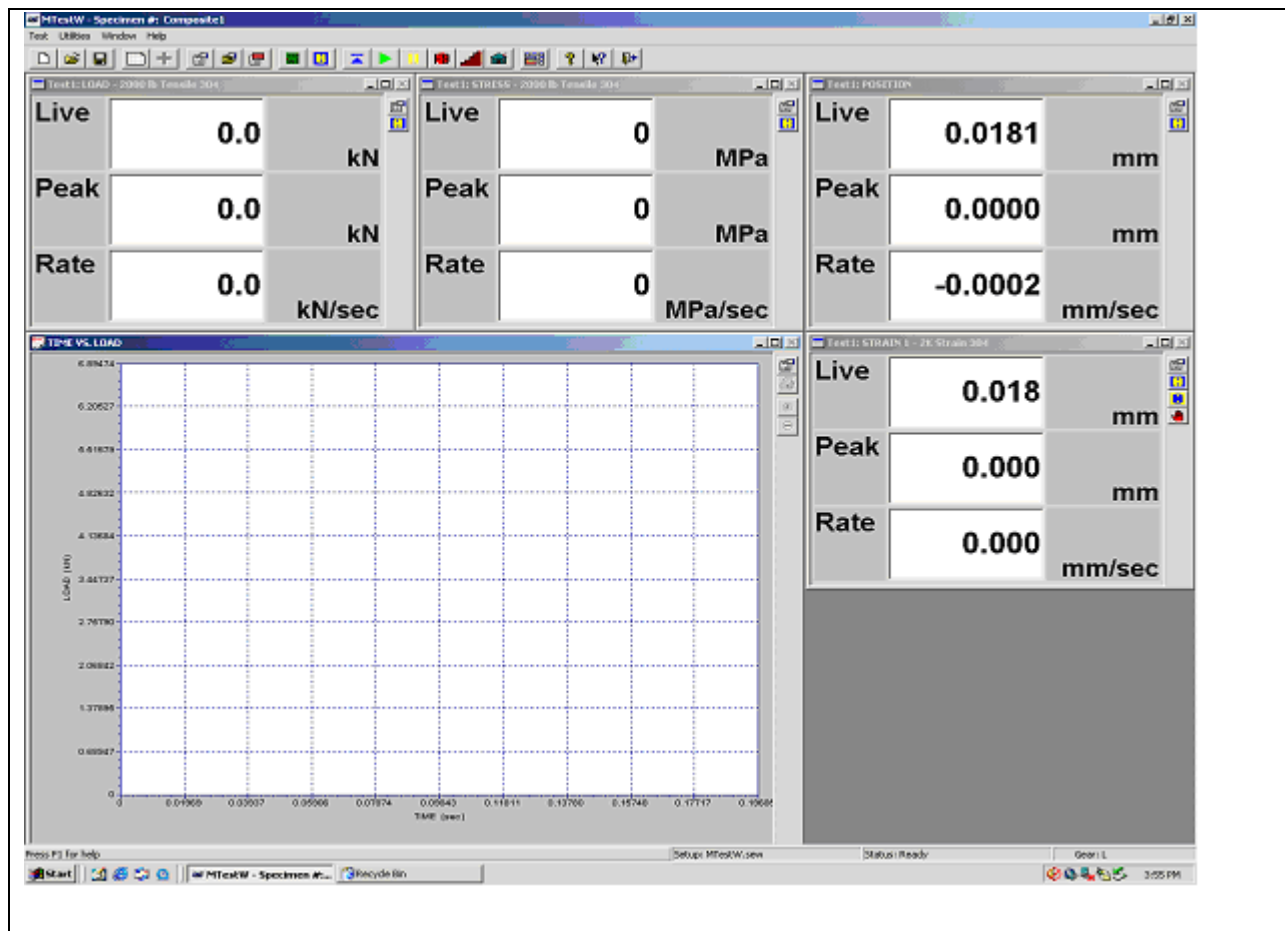

Figure 3.4 Typical Screen of the MTest Windows Software.

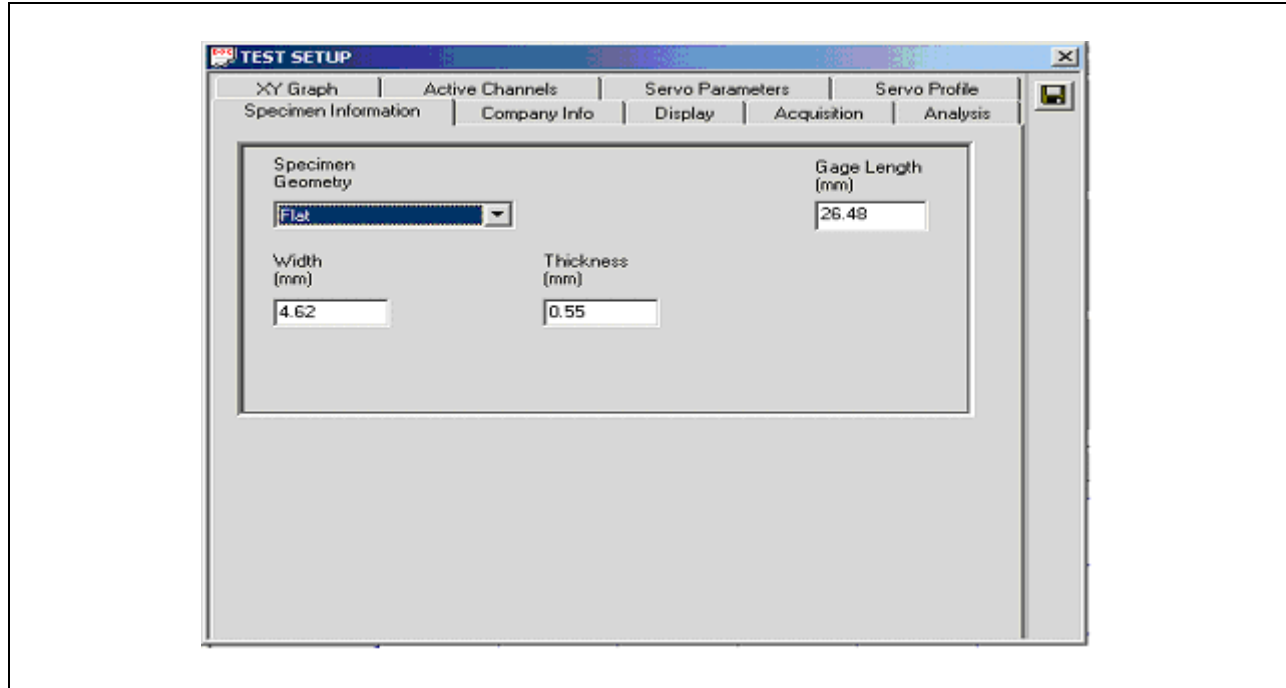A typical test setup menu is depicted in Figure3.5

Figure3.5 Screen Shot of Test Setup Menu.

In the test setup window clicking on the display button gives options to display load, stress, length and time in desired units.

In the servoparameters option, as shown in Figure 3.6, the preload, preload rate, jog speed, home rate and the port test are fixed. The preload amount and the preload rate are used to apply small load to the specimen prior to the starting of the test. This preload amount should be less than start test threshold. The jog speed is the rate at which the crosshead moves while loading the specimen. The home rate is the rate at which the machine will return to its starting zero position when the home icon is clicked. Post test action defines the movement of the cross-head after the end of the test is detected. In the present testing, the stop option is selected for the post test action so as to not reverse load on the substage after testing; Very high loads could affect the load cells.
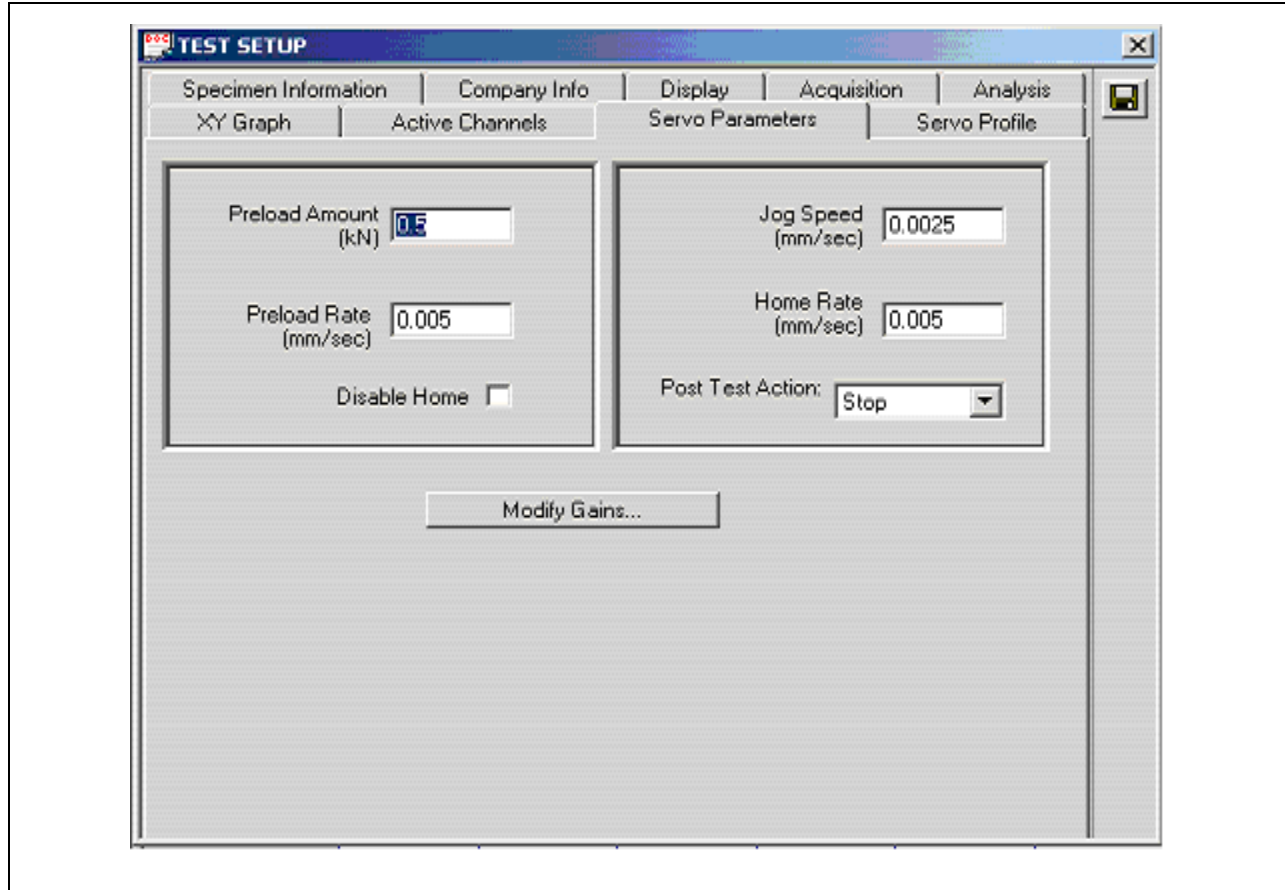
Figure 3.6 Screen Shot of Servoparamaters Window.

The acquisition menu shown in Figure 3.7 allows fixing parameters such as sample brake, threshold load and segmenting log rate. Sample brake is the load at which failure of the present specimen is detected by the substage and to stop the testing. For the present test the specimen break is set at 20% of the peak load of the specimen. Threshold load is the load at which the program starts logging in data. The threshold rate should always be set higher then the preload. Finally, the segment log rate and segment duration defines the frequency and the length that the data is being logged. Most of the parameters are fixed and rarely change other then specimen information and the servoparameters.
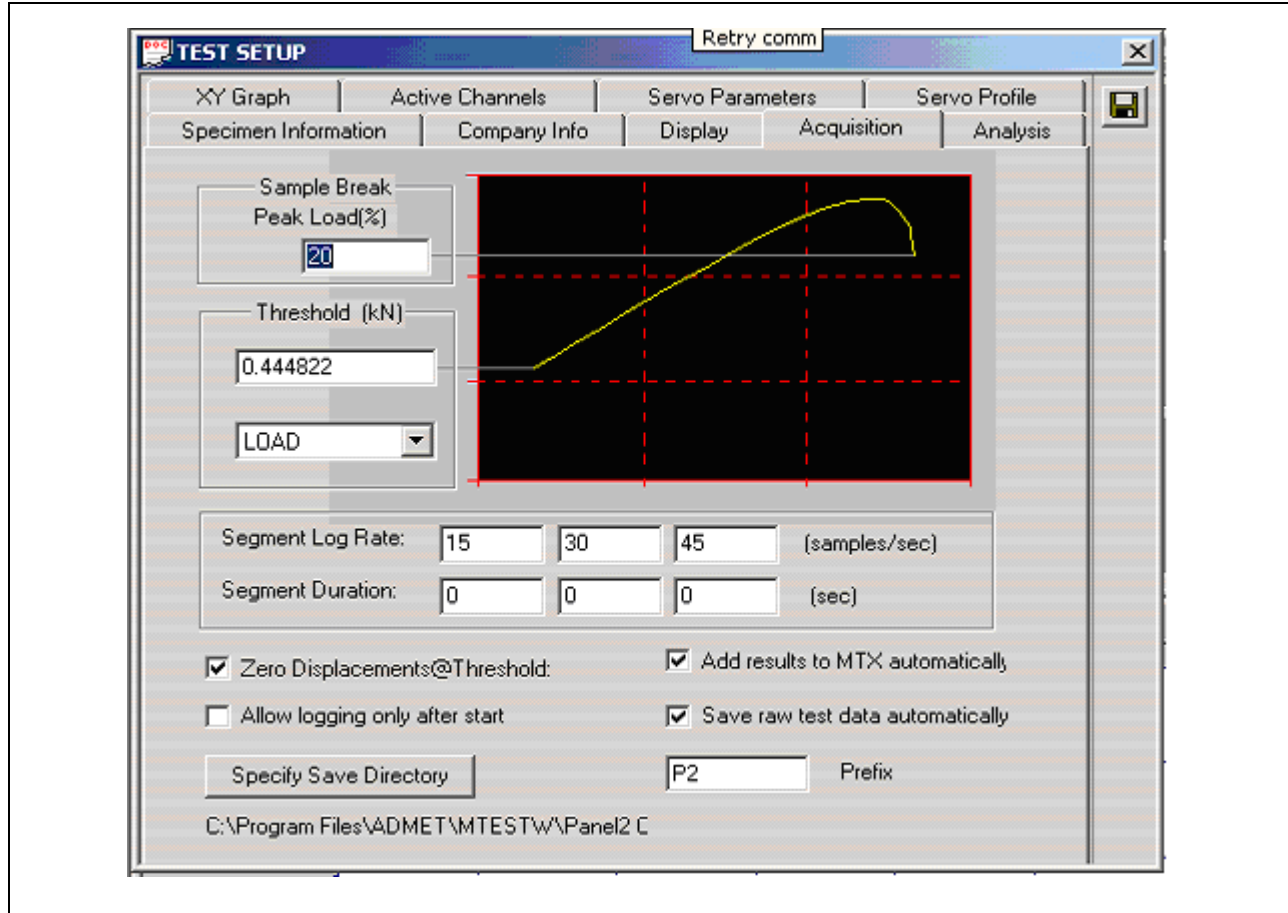
Figure 3.7 Screen shot of Acquisition Menu.

3.4 Optical Microscopy

Optical microscopy was performed using a ProScope digital USB microscope with a 200X magnification lens. The still capture capability of the microscope was 640x480 (VGA) pixels. The microscope was mounted on a stand parallel to the substage so as to focus on the surface developing microcracks. The stand of the microscope has a micrometer which facilitated (1) the movement of the microscope to and fro parallel to the surface under investigation and (2) the measurement of the distance moved. For the current testing, the typical in-focus span across the specimen was between 10 mm to 14 mm. For clarity, this distance across the specimen in which

the micrographs are obtained will be referred to as the optical span length. A high intensity illuminator was used to brighten the surface under investigation to get good results. Figure 3.8 is a picture of the optical microscopy setup.
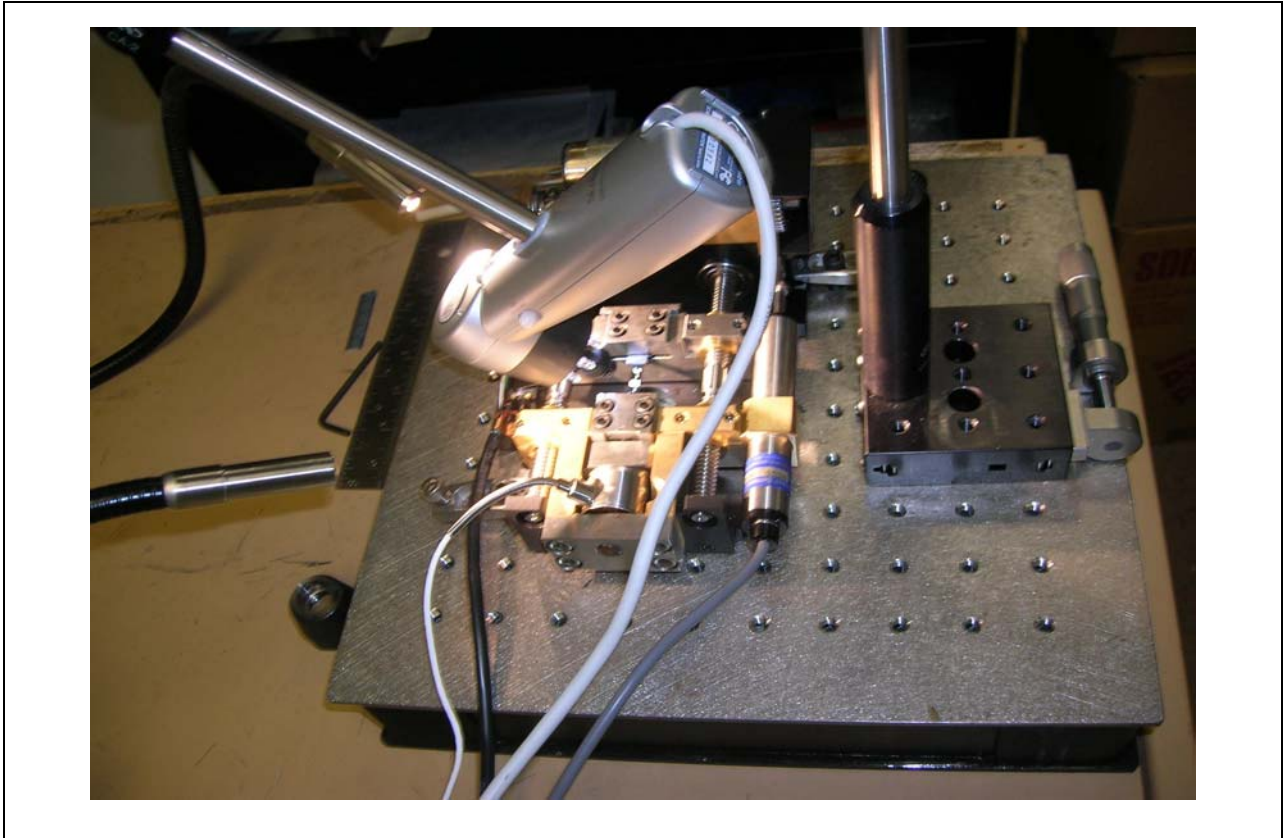

Figure 3.8 Optical Microscope Setup.

3.5 Experimental Procedure

The acquisition system is turned on and it is made sure the acquisition system is in tension mode by using the switch on the data acquisition system. After the above procedure the acquisition system is turned on and it is made sure the acquisition system is in tension mode by using the switch on the data acquisition system. Then the MtestWindows software is turned on.

The clamps of the substage are designed with two self adjusting wedge shaped grips to make a smooth tightening of the clamps. After the specimen is placed between the clamps, they are hand-tightened and the distance between the clamps was measured using a digital caliper. This distance is taken as the gauge length. For a typical specimen the gauge length was around 25mm. Then the test setup icon is opened from the file pull-down menu in the MTest Windows software. The desired specimen information is input using the specimen information window. The parameters for the present testing used were flat specimen, gauge length, width and thickness. After the specimen information is entered the servoparameters are fixed. The servoparameter settings for the present study is 0.0025 mm/sec for the jog speed, 0.005 mm/sec for the home rate, 0.5 KN for the preload, and the post test is set to stop.

The above test set-up is saved by the name of the specimen and the screws of the clamps are tightened. After tightening the specimen the stress and the load induced on the specimen are noted to make sure the clamping stress and load not to exceed the preload.

Then the optical microscope is focused on the surface at one end and moved to the other end noting the span of focus of the microscope and best visualization of the surface throughout the specimen. Then the specimen is loaded, stopped at pre-determined stress intervals, and inspected using optical microscopy for microcracks. For the specimens in the present test, specimens are loaded to 750MPa continuously and then stopped at every 50MPa interval. At each of these loadings snap shots of the surface are taken. The field of view in each optical micrograph covers a 1.375mm specimen length. After grabbing the first snap shot the micrometer is translated in increments of 1.25mm until the total travel of the micrometer is between 10 and 14mm (This

length is dependent on the length of the specimen). An optical micrograph is taken at each increment of micrometer travel. A 10mm micrometer travel results in a total optical scan length of 11.375 mm.

3.6 Microcracks and Distance Measurements

As previously noted, the specimen length in the field of view of a single micrograph is 1.375mm. Each of these images is captured with 640 horizontal and 480 vertical pixels. The snapshots from each stress level are grouped together and the number of microcracks for the optical scan length is counted. Note that this process is a bit tedious since there is an overlap length of 0.125mm between consecutive micrographs. Then by using a zooming software tool, ZoomMagic, the number of pixels between each crack is determined. Figure 3.9 displays a typical optical micrograph and Figure 3.10 displays the screen shot of the ZoomMagic software.
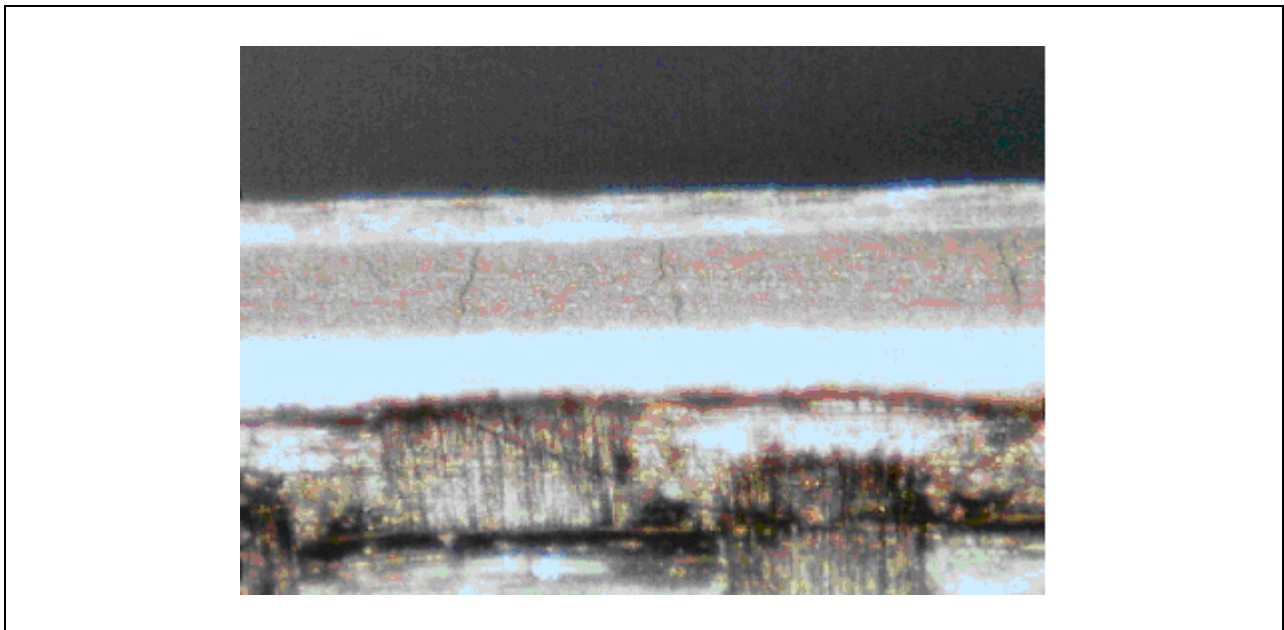
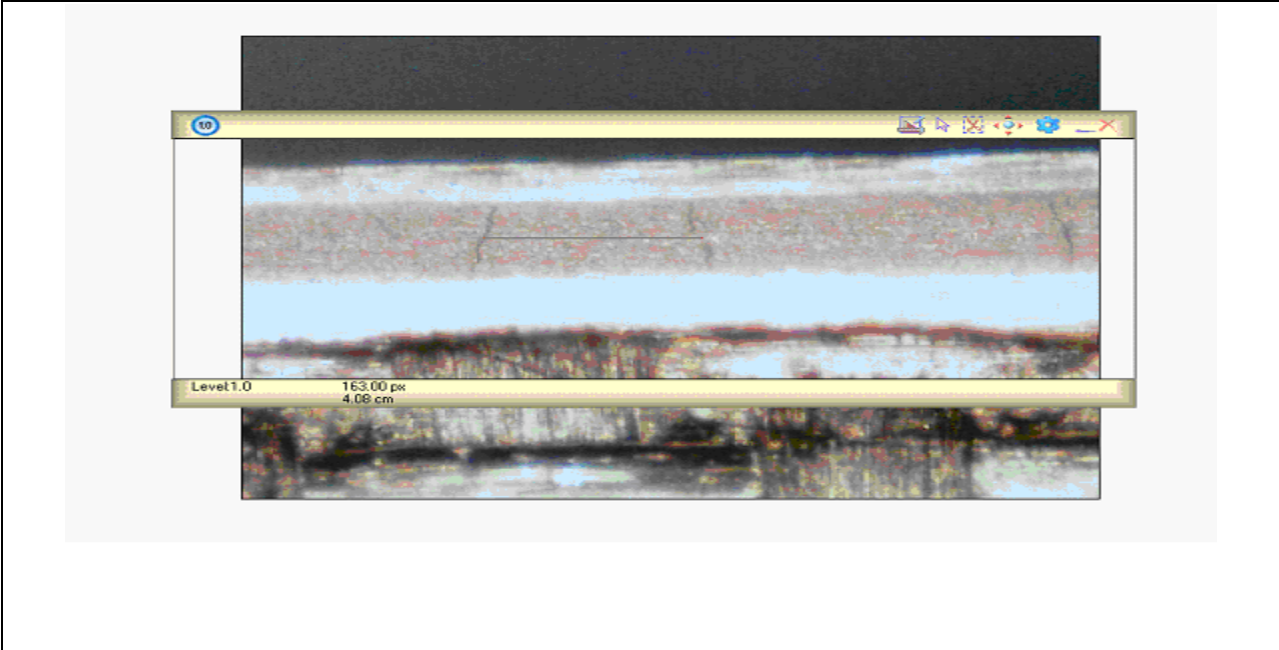

Figure 3.9 Optical Micrograph

Figure 3.10 Screen Shot of ZoomMagic Software.

4. Results

The experimental procedure was followed as described in the previous chapter. Accordingly, data for the IM7/977-2 material system specimens listed in Table 3.1, the IM7/5555 material system specimens listed in Table 3.2, and the IM7/5276-1 material system specimens listed in Table 3.3 are presented in this section. For each material system, at least six of the specimens were tested up to failure. In some cases, the specimens were loaded in the vicinity of, but not up to, the failure load to explore the failure behavior of the material systems. For each material system, optical microscopy was performed to gather microcrack initiation and propagation data as well as to investigate the damage progression in the different systems. From all the specimens loaded to failure optical microscopy was performed and the spacing between each microcrack was measured. The various results are discussed in following sections.

4.1 IM7/977-2: Microcracking and Damage Progression

Table 4.1 lists the optical scan length, the crack initiation stress, the maximum stress induced in the specimen, the maximum crack density, and whether or not the specimen was loaded to failure. The specimens failed at different loads, with 1133MPa being lowest failure load and 1332MPa being the highest failure load. The average failure load of the IM7/977-2 material system was found to be around 1220MPa.

Table 4.1 Microcracking and Load Data for Material System IM7/977-2.

Specimen	Optical Span Length (mm)	Crack Initiation Stress (MPa)	Crack Density (Cracks/cm)	Maximum Stress (MPa)	Failure
2-I-II-5	10.125	1029	2.0	1133	Yes
2-I-II-6	11.375	1015	7.9	1222	Yes
2-I-II-7	11.375	1005	6.2	1266	Yes
2-I-III-1	13.875	1054	11.5	1322	Yes
2-I-III-3	11.375	1026	10.5	1208	Yes
2-I-III-9	10.125	1065	5.9	1180	Yes
2-I-III-4	13.875	1014	Test Stopped	1151	Stopped
2-I-III-5	11.375	1056	Test Stopped	1156	Stopped

Figures 4.1 through 4.6 depict the schematics of the crack formation for each specimen at incremental loadings for the specimens that failed. From the schematics it can be seen that the microcracks did not initiate in the in the center of the optical scan of the specimen. This may be due macroscopic flaws in the material in that area and imperfections in the specimen. After the initial formation, new cracks initiated between the existing microcracks. The maximum number of 16 cracks was observed in specimen 2-I-III-1 at 1296MPa for an observable span of 13.875mm, which resulted in a crack density of 11.5cracks/cm. This material system did not show a clear indication of microcracking saturation. This is may be due the fact that at higher loads the energy was expelled due to other forms of failures, such as delamination, fiber pull-outs, etc

While microcracking initiated in the IM7/977-2 material system at loads around 1000MPa, other types of damage were observed under the optical microscope prior to total failure. Table 4.2 presents a discussion regarding the damage occurring in each specimen. Delamination was not observed in all of the specimens up to within 50 MPa of the failure loads, with the exception of specimen 2-I-III-3. For the other two specimens (2-I-III-1 and 2-I-III-9) in which delamination was observed, the specimens failed immediately after applying a load of 20-25MPa.
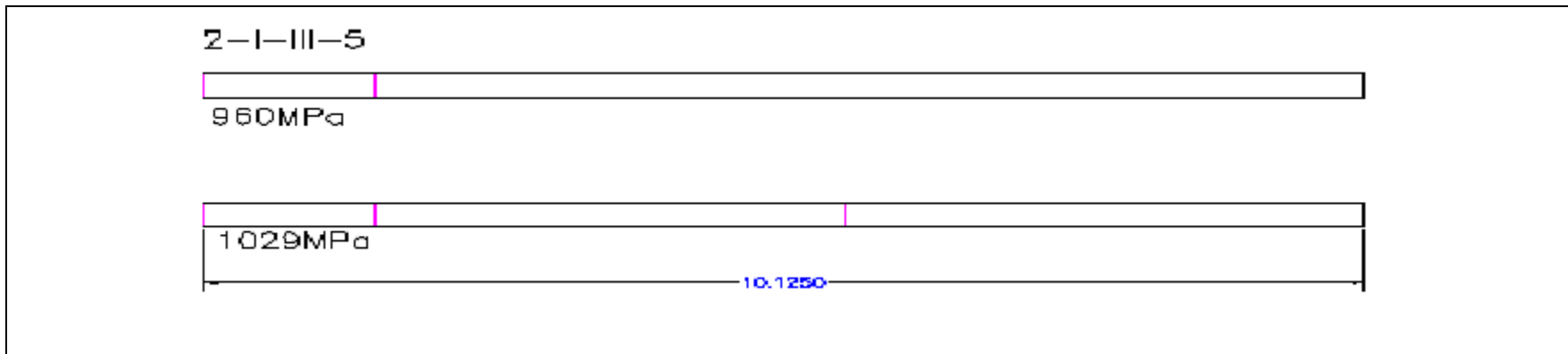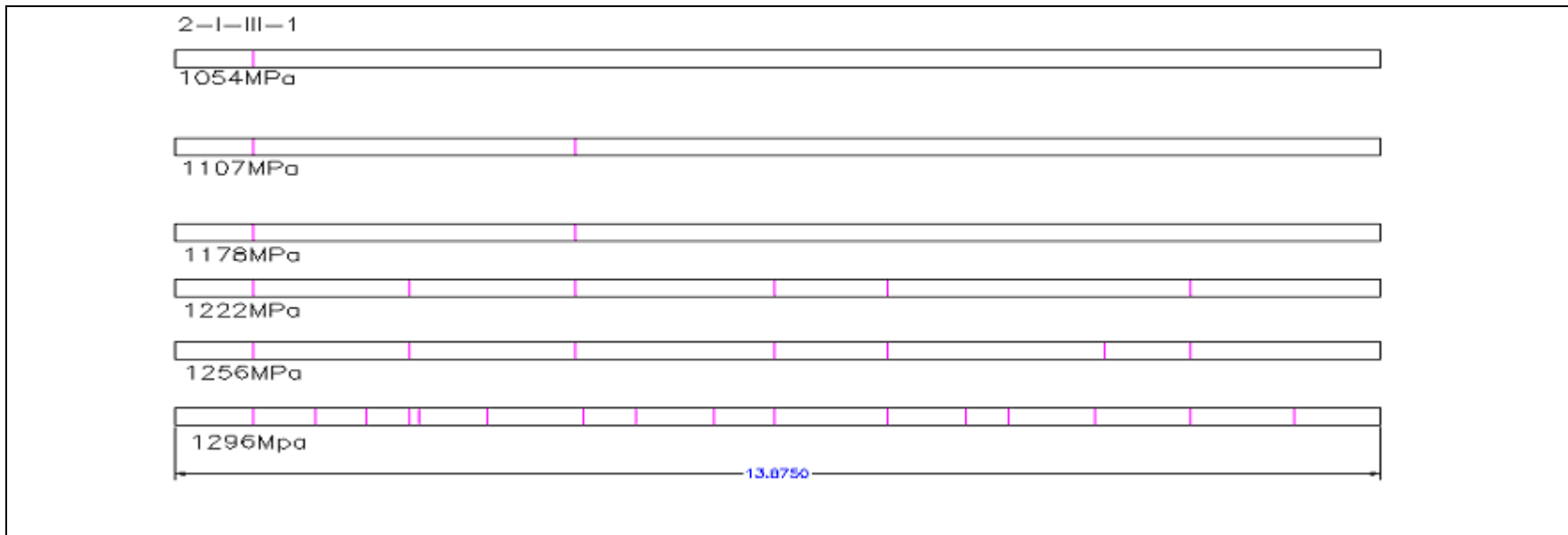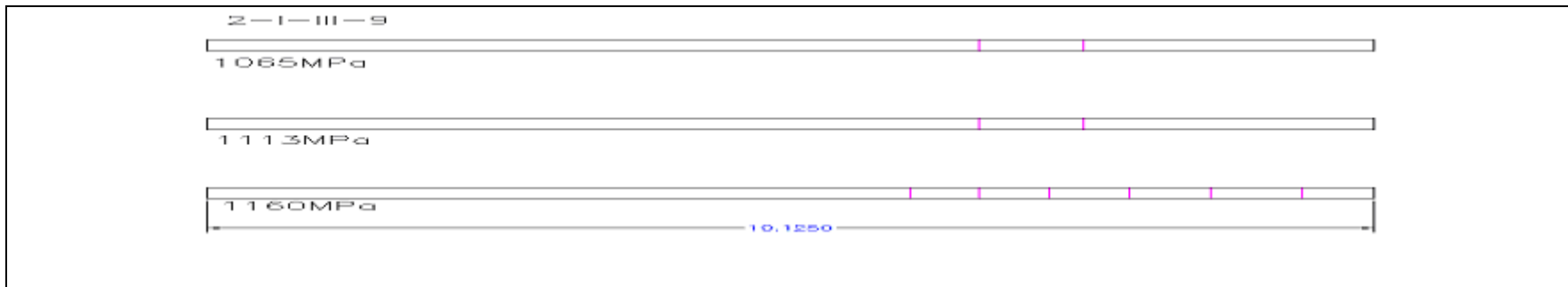
Figure 4.1 Schematics of Crack Propagation in Specimen 2-I-III-5.
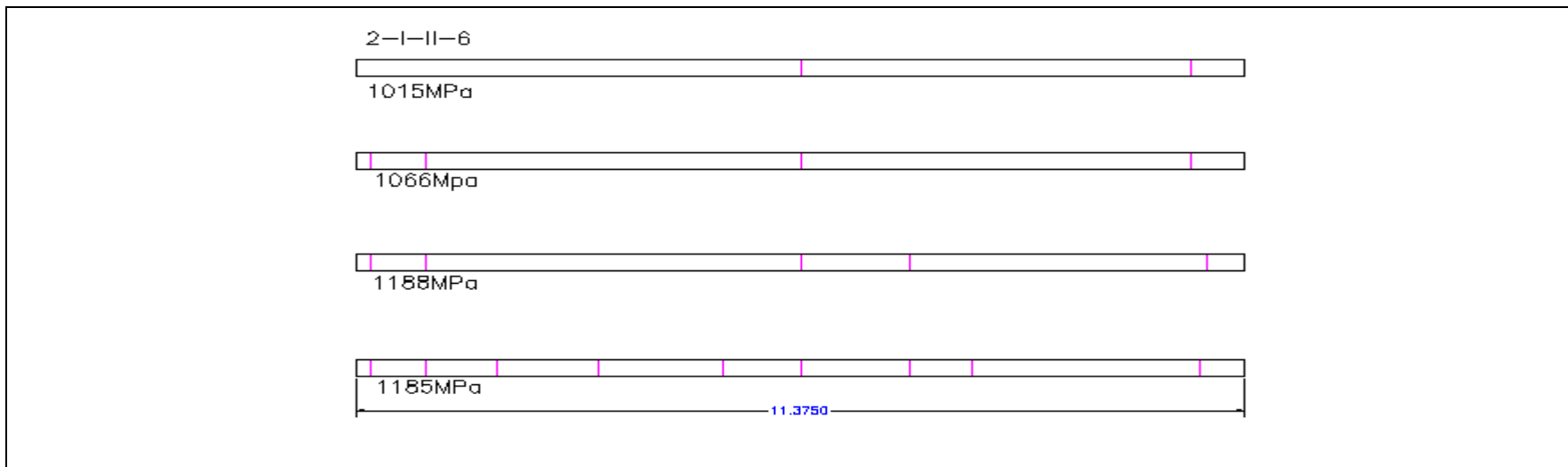
Figure 4.2 Schematics of Crack Propagation in Specimen 2-I-III-6.

29
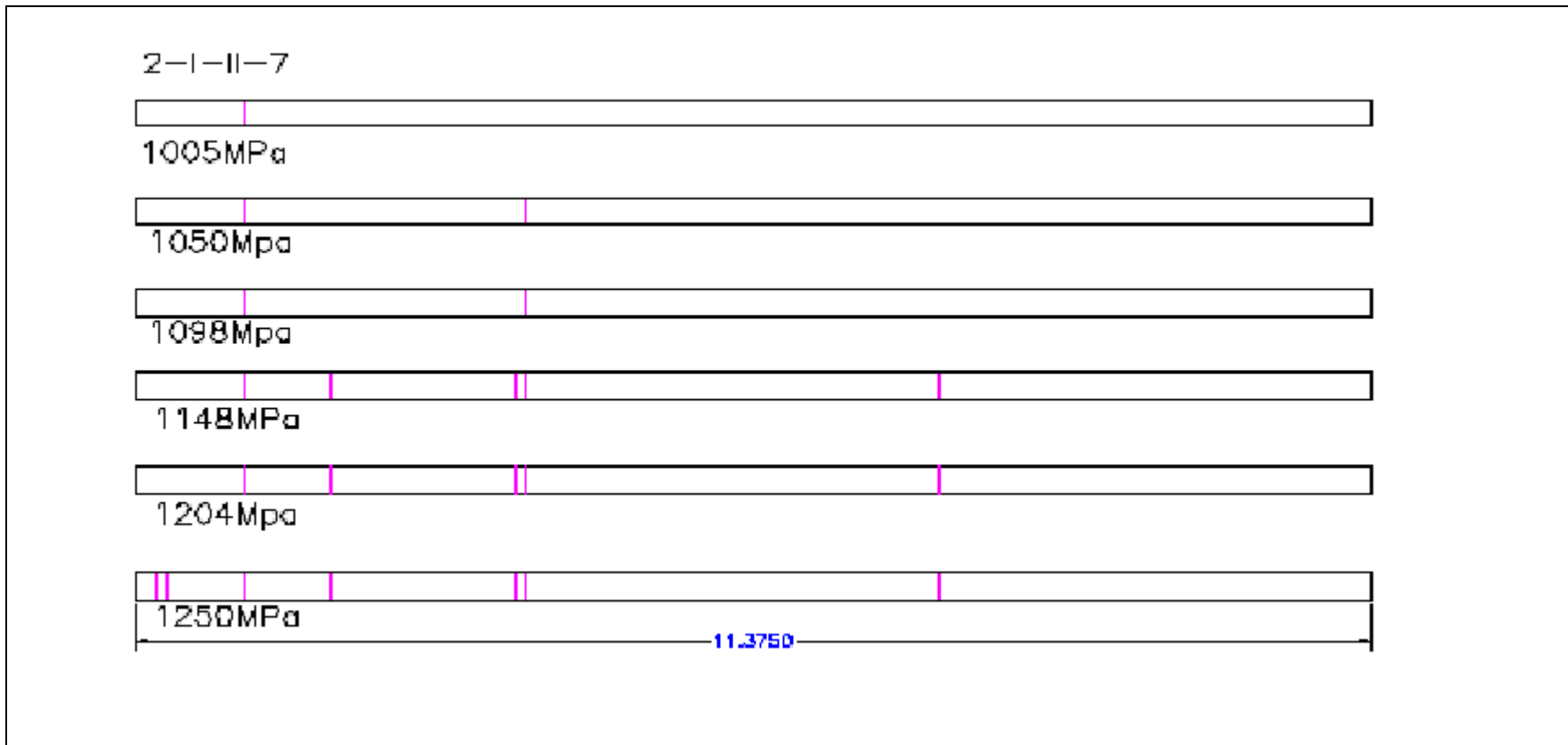
Figure 4.3 Schematics of Crack Propagation in Specimen 2-I-II-7.

Figure 4.4 Schematics of Crack Propagation in Specimen 2-I-III-1.

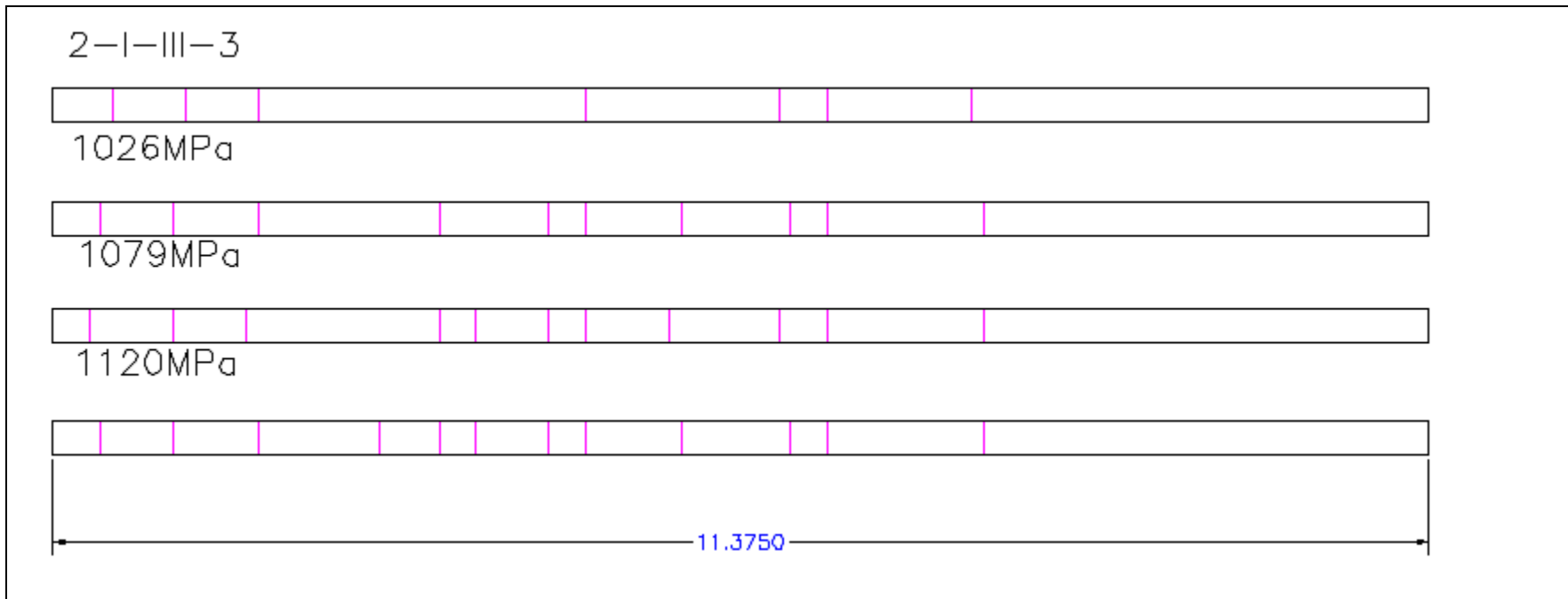*Figure 4.5 Schematics of Crack Propagation in Specimen 2-I-III-9.*
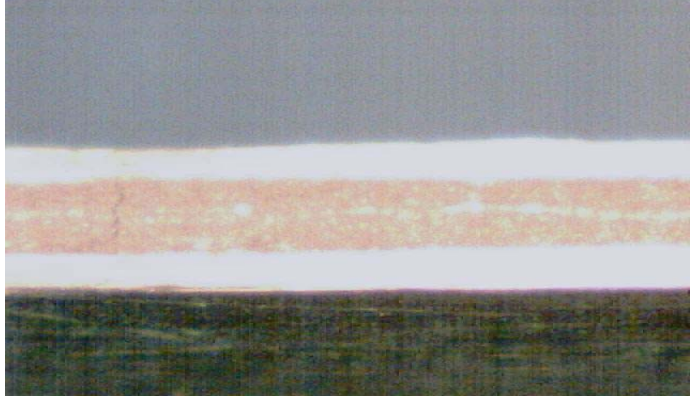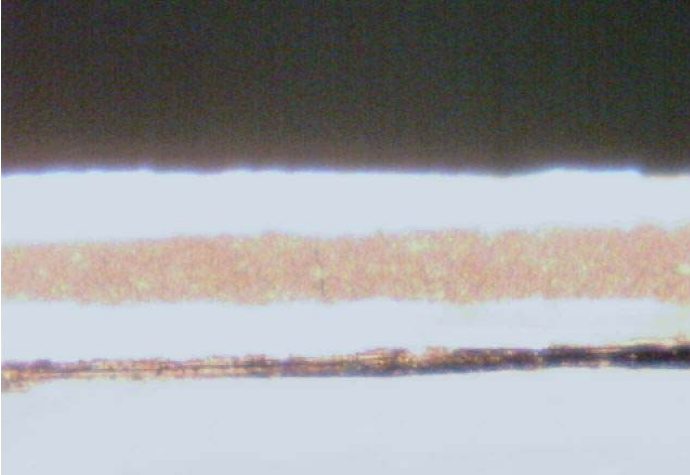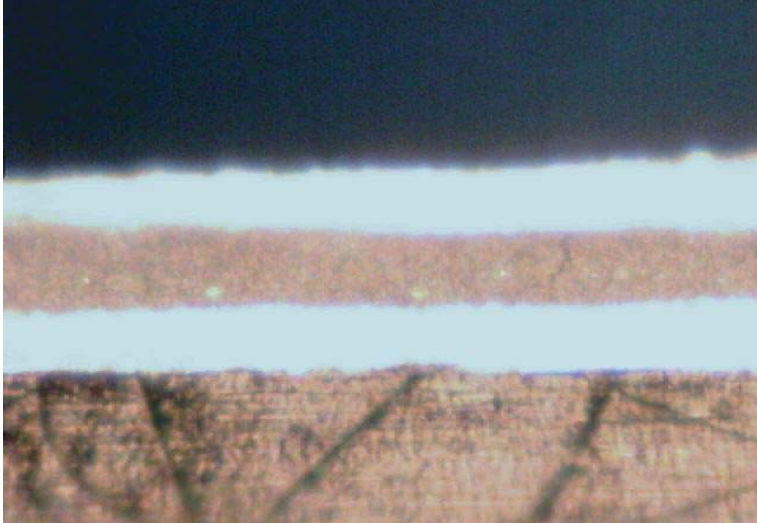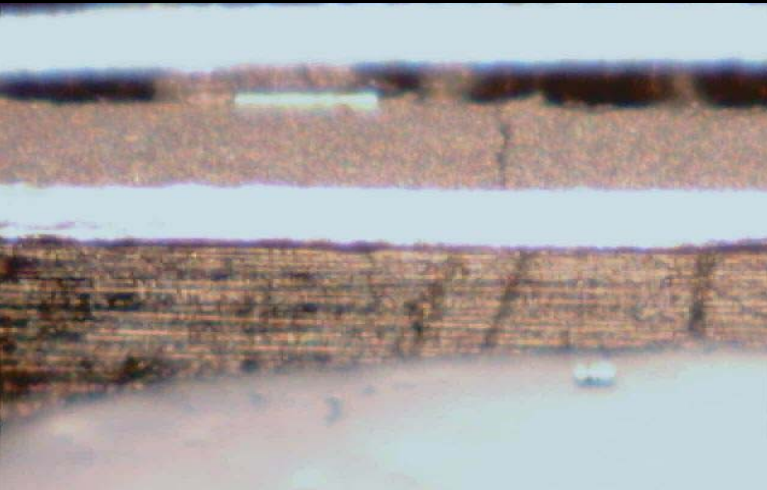
31

Figure 4.6 Schematics of Crack Propagation in Specimen 2-I-III-3.

Table 4.2 Micrograph Observations for Material System IM7/977-2.

Specimen	Micrograph	Damage Load (MPa) and Discussions
2-I-II-5		Specimen 2-I-II-5 did not show any other form of other damage under optical microscope and the specimen failed at 1133MPa. The picture in the left shows the micrograph with a single microcrack at 1087MPa. The specimen failed near the tabs.
2-I-II-6		Specimen 2-I-II-6 did not show any other form of other damage under the optical microscope and the specimen failed at 1222MPa. The picture in the left shows the micrograph with a single microcrack at 1185MPa. The specimen failed into two pieces in the mid span.

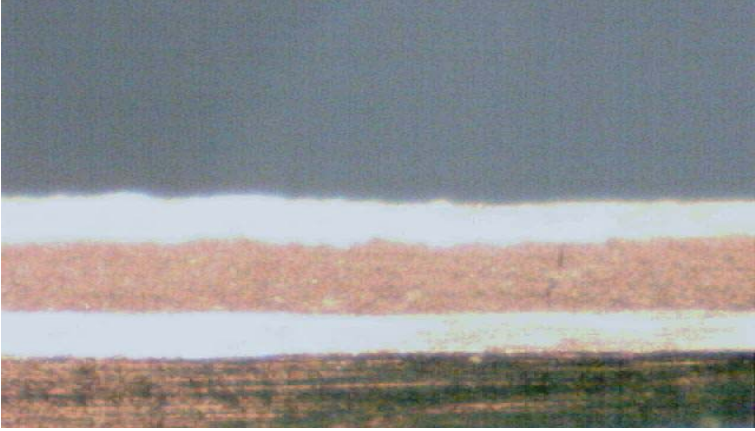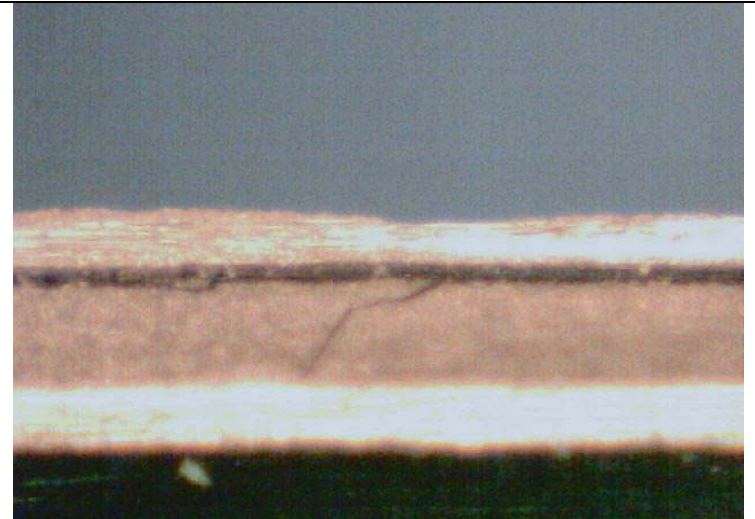|		
2-I-II-7		Specimen 2-I-II-7 did not show any kind of other damage before failure. The specimen failed at a load of 1266MPa. The specimen failed near the tabs. The micrograph in the left shows the micrograph at the load of 1250MPa.
2-I-III-1		The micrograph to the left is from specimen 2-I-III-1 at 1297MPa. Delamination was observed at a load of 1297MPa. The specimen failed at the ends of the tabs with additional load of 25MPa.

2-I-III-3	 	The micrographs in the left are from specimen 2-I-III-3 at load of 1026MPa and 1172MPa. It can be seen that there are two microcracks in both micrographs. Delamination was observed at a load of 1026MPa. The specimen failed at a load of 1208MPa. In the top picture and as the load increases the delamination increases between the 0° ply and 90° plies.

| 2-I-III-9 | | The figures in the left show the micrograph of specimen 2-I-III-9 at loads of 1113MPa (top) and 1160MPa (bottom). At 1113MPa no other form of damage was observed other then a single microcrack. At 1160MPa the specimen started delaminating between the 0° plies and 90° plies in the upper ply group. Fiber pull-out in the lower ply group between the 90° and 0° plies was also observed. There is also an additional new microcrack and they both provide contact delamination. This specimen immediately failed into two pieces at an additional load of 20MPa. |

2-I-III-4		Specimen 2-I-III-4 did not show any other forms of damage under the optical microscope. The test was stopped at 1151MPa.
2-I-III-5		Specimen 2-I-III-5 started to delaminate at a load of 1156MPa, as seen in the micrograph. The test was stopped.

4.2 IM7/5555: Microcracking and Damage Propagation

Table 4.3 lists the optical scan length, the crack initiation stress, the maximum stress induced in the specimen, the maximum crack density, and whether or not the specimen was loaded to failure for the IM7/555 specimens.

Table 4.3 Microcracking and Load Data for Material System IM7/5555.

Specimen	Optical scan length (mm)	Crack Initiation Stress (MPa)	Crack Density (Crack/cm)	Maximum Stress (MPa)	Failure
5-I-II-1	11.375	871	11.4	1206	Yes
5-I-II-2	11.375	876	16.7	1316	Yes
5-I-II-3	11.375	893	13.2	1352	Yes
5-I-II-5	11.375	884	16.7	1495	Yes
5-I-IV-1	11.375	818	16.7	1311	Yes
5-I-IV-3	11.375	855	16.7	1304	Yes
5-I-IV-8	13.875	873	16.7	1256	Stopped
5-I-I-3	11.375	984	10.1	1264	Stopped

The IM7/5555 material system failed at higher loads than that of IM7/977-2. The maximum failure stress reached was 1495MPa and the lowest failure stress reached was 1206MPa. The average failure stress for the six specimens tested to failure was found to be around 1330MPa.

As can be seen from Table 4.3, five of the specimens reached a crack density of 16.7cracks/cm. It can also be noted that specimens 5-I-IV-1, 5-I-IV-3, and 5-I-IV-8 were cut from the same

location of the initial panel and they all reached the same crack density. For the six specimens loaded up to failure the average crack density at failure was found to be 15.2cracks/cm. In all of the samples, with the exception of 5-I-I-3, microcrack initiation was observed at around the load of 850MPa.

Figures 4.7 through 4.12 display schematics of crack formation for six IM7/5555 specimens tested to failure. All the specimens had an optical span length of 11.375mm under the optical microscope. The material system IM7/5555 started microcracking in the mid-span of the specimen, as expected. Five of the specimens displayed the same number of maximum microcracking in the span of 11.375mm resulting in a crack density of 16.7cracks/cm. The cracks were more evenly distributed throughout the length of the specimen than those of the IM7/977-2 specimens.
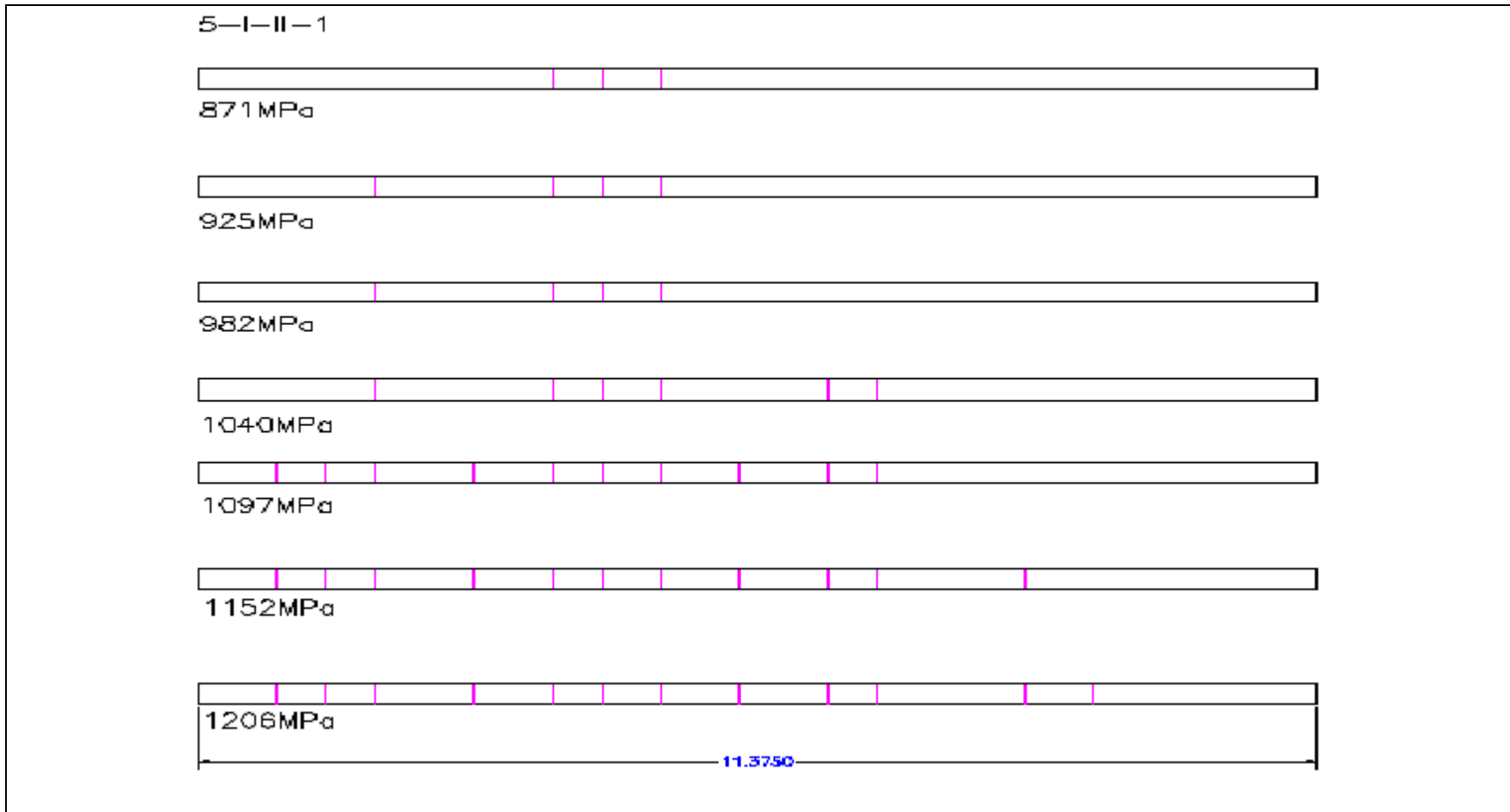
Figure 4.7 Schematics of Crack Propagation in Specimen 5-I-II-1.

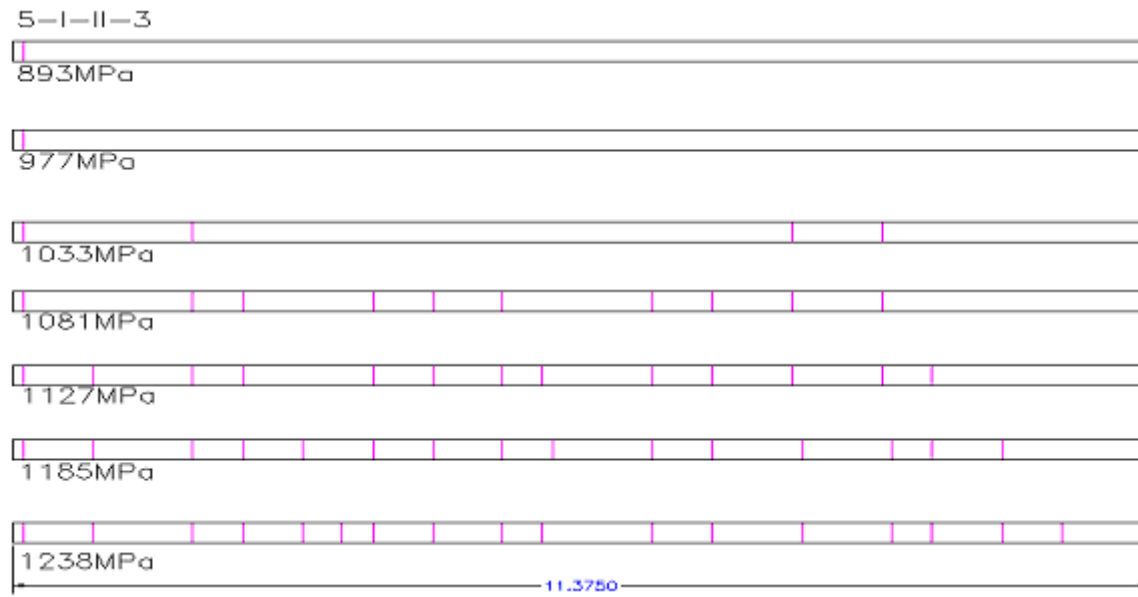*Figure 4.8 Schematics of Crack Propagation in Specimen 5-I-II-2.*

Figure 4.9 Schematics of Crack Propagation in Specimen 5-I-II-3.
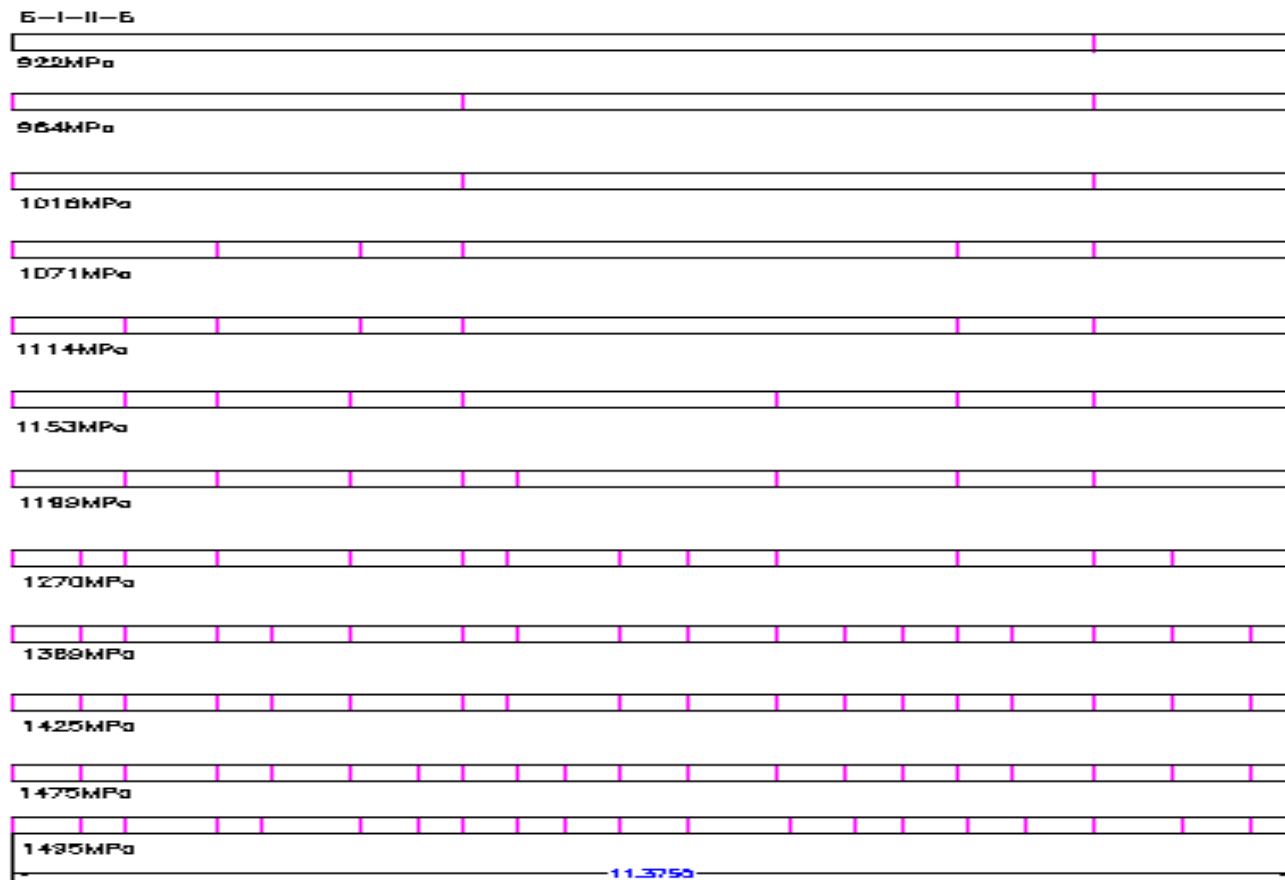
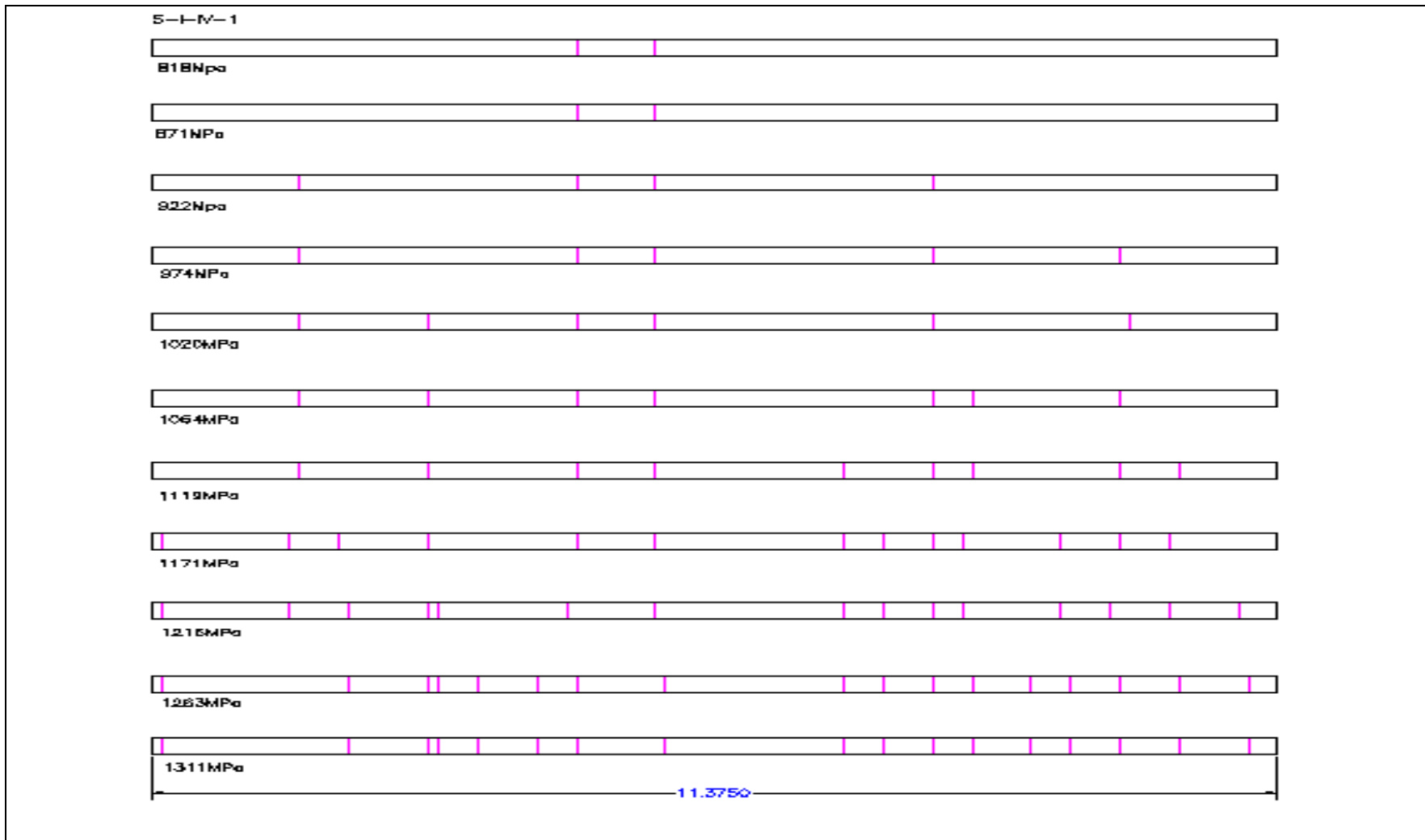*Figure 4.10 Schematics of Crack Propagation in Specimen 5-I-II-5.*

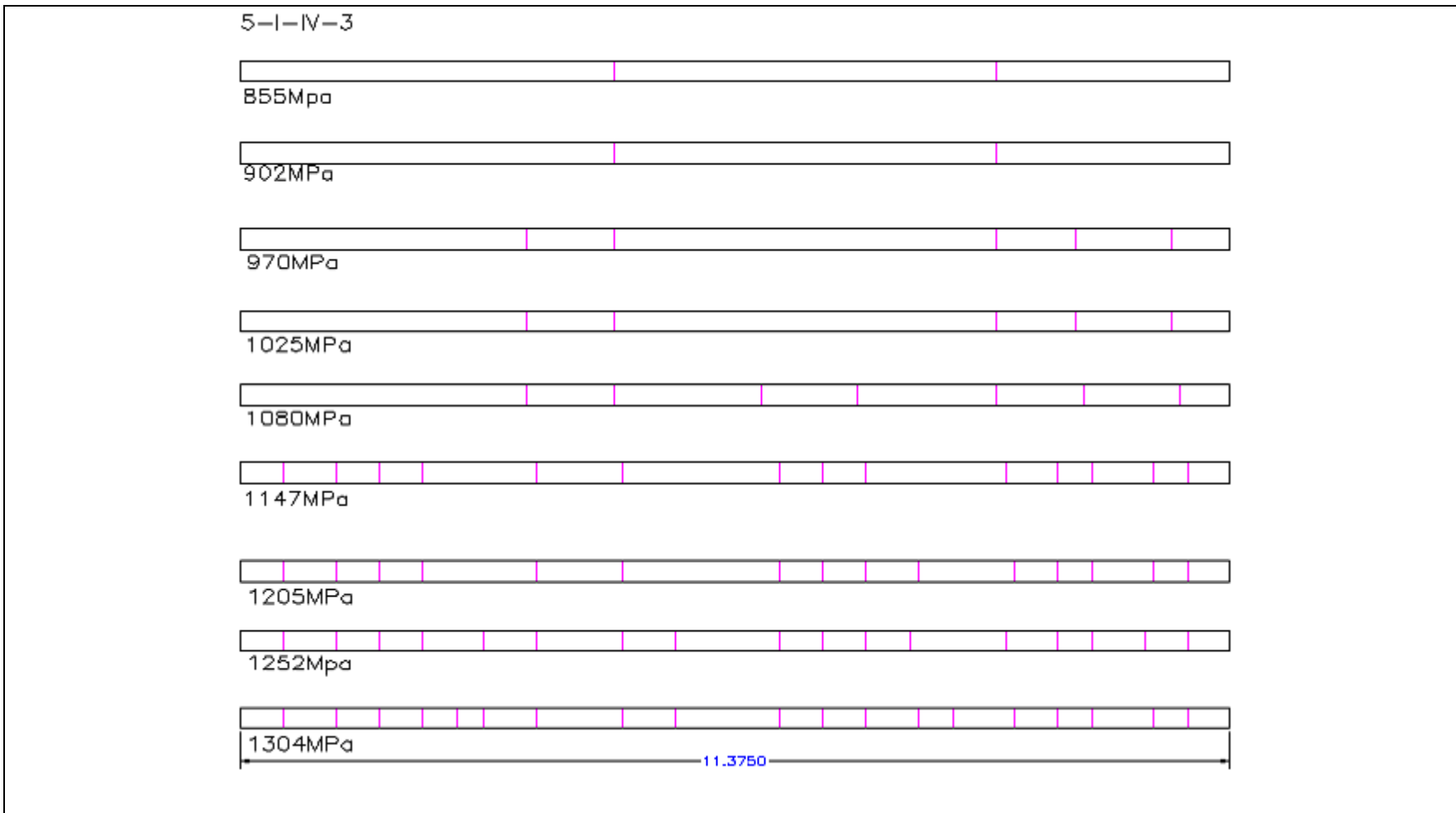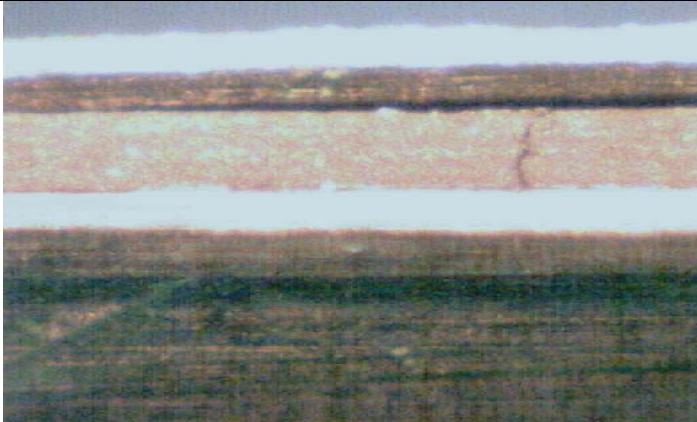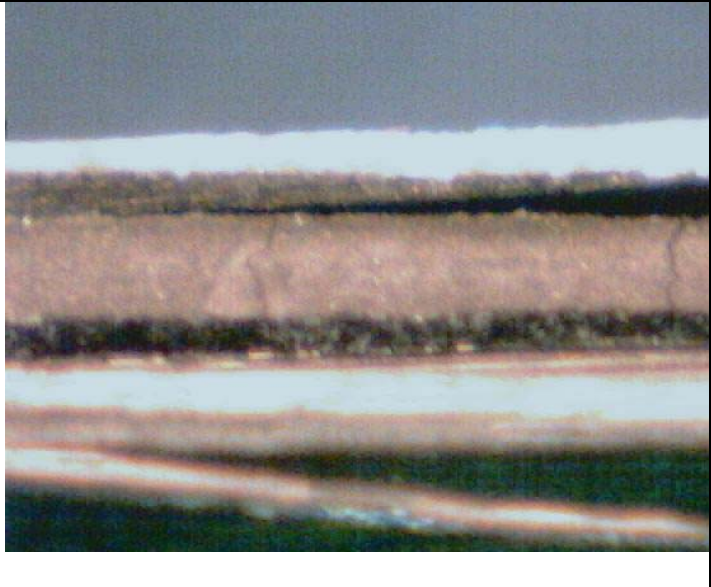*Figure 4.11 Schematics of Crack Propagation in Specimen 5-I-IV-1.*
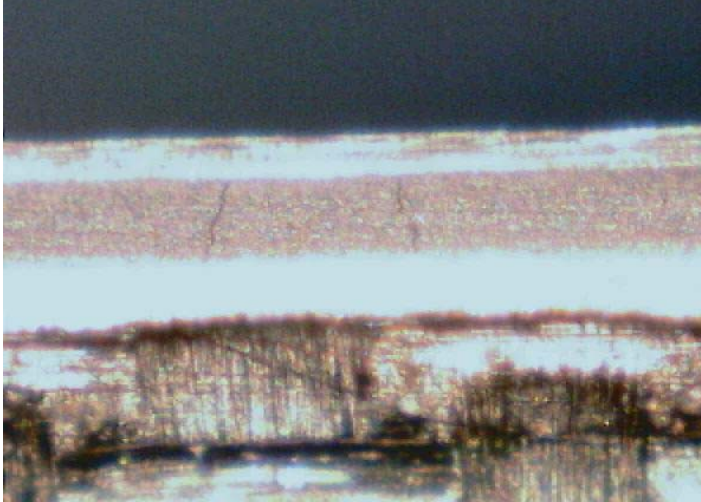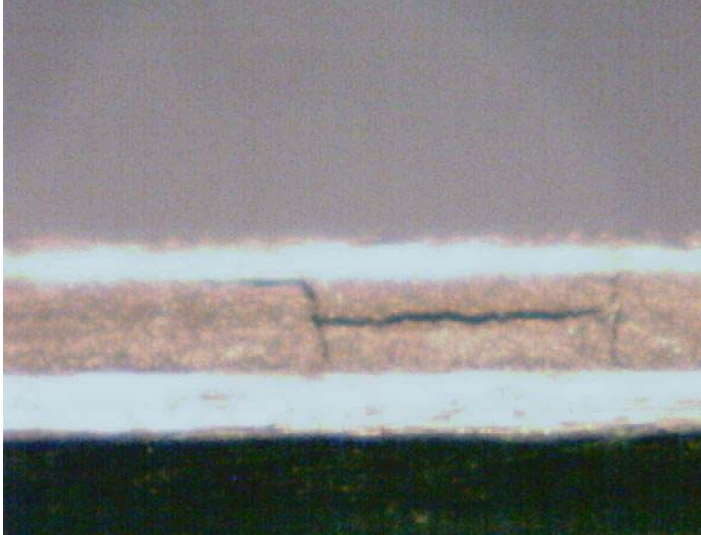
Figure 4.12 Schematics of Crack Propagation in Specimen 5-I-IV-3.
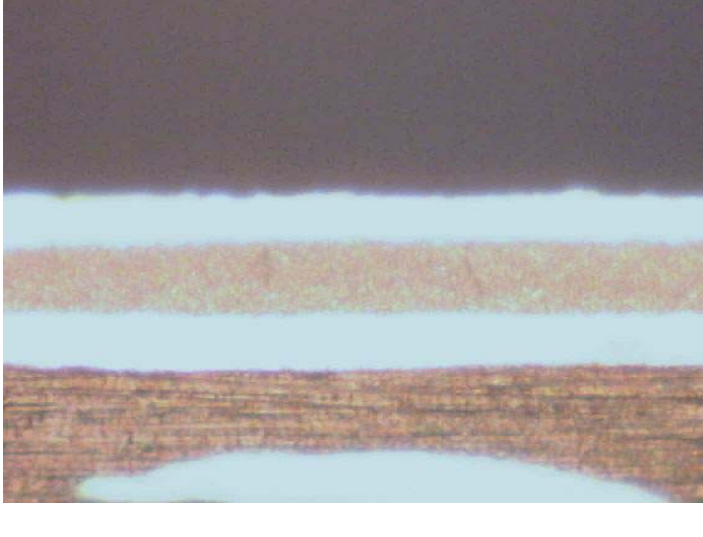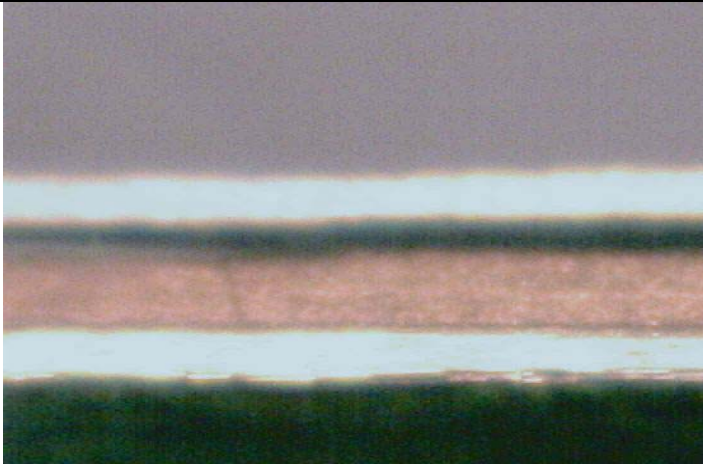
After the initial formation of microcracks, at around 850MPa, the material system did display other kinds of damage, like delamination and fiber pull-out. Table 4.4 displays and discusses the damage progression. Delamination was observed in five specimens at loads between 1000MPa and 1100MPa. Among these five specimens, three of these specimens had microcracking density around 10cracks/cm upon delamination. From this observation it can be inferred that the material system IM7/5555 starts delaminating around 10 cracks/cm and stress levels around 1050MPa, with total failure occurring around 1330MPa. A second observation that can be made is that material system IM7/5555 can absorb more energy and can go up to higher stress levels even after delamination occurs.

Table 4.4 Micrograph Discussions for Material System IM7/5555.

Specimen	Micrograph	Damage Load(MPa) and Discussions
5-I-II-1		The micrograph is taken at a load of 1206MPa. Delamination was observed in the specimen at a load of 1040MPa. The specimen broke into pieces at failure.
5-I-II-2		The micrograph is taken at a load of 1316MPa. It can be seen from the micrograph there is fiber pull-out and delamination between the 90° plies and the 0° plies. Delamination was observed in the specimen at the load of 1021MPa. The specimen failed into pieces at failure.

| 5-I-II-3 | | This is taken at a load of 1352MPa. It can be seen from the micrograph, there is fiber pull-out and delamination in the specimen.   Delamination was observed in the specimen at a load of 1081MPa.The specimen failed into pieces. |
| 5-I-II-5 | | The micrograph was taken at a load of 1495MPa. In the micrograph it can seen the specimen developed fiber pull-out in the edges of the specimen and the specimen failed into pieces at failure. |

5-I-IV-1		The micrograph was taken at a load of 1304MPa. The specimen developed 3 microcracks at this location. The micrographs did not show other kind of damage before failure. At failure, the specimen into broke into pieces.
5-I-IV-3		The micrograph was taken at a load of 1311MPa. The specimen developed delamination between the two 90° plies and some delamination in other locations between the 0° plies and 90°. This specimen failed immediately into pieces.

5-I-IV-8		The micrograph was taken at a load of 1264MPa. The micrograph depicts showing 2 microcracks and one half microcrack. The micrographs did not show other kinds of damages before the test was stopped at 1264MPa.
5-I-I-3		The micrograph was taken at a load of 1264MPa. Delamination was observed at the load of 1026MPa. The test was stopped at 1264MPa.

4.3 IM7/5276-1: Microcracking and Damage Propagation

Table 4.5 lists the optical scan length, the crack initiation stress, the maximum stress induced in the specimen, the maximum crack density, and whether or not the specimen was loaded to failure for the IM7/5276-1 coupons.

Table 4.5 Microcracking and Load Data for Material System IM7/5276-1.

Specimen	Optical scan length (mm)	Crack Initiation load (MPa)	Crack Saturation Density (Cracks/cm)	Maximum Stress(MPa)	Failure
6-II-IV-1	10.125	932	7.9	1278	Yes
6-II-IV-2	10.125	1004	7.9	1345	Yes
6-II-IV-4	10.125	1010	12.8	1381	Yes
6-II-IV-5	11.375	983	14.8	1349	Yes
6-II-IV-6	11.375	870	11.4	1202	Yes
6-II-IV-7	13.875	852	10.1	1160	Yes
6-II-IV-3	10.125	950	10.9	1357	Yes

The specimens failed at different loads, with 1160MPa being the lowest failure load and 1381MPa being the maximum failure load. The average failure stress for the seven specimens from material system IM7/5276-1 was found to be around 1290MPa. Figures 4.13 through 4.18 display the schematics of the crack formation of the six specimens at different loads.

Figure 4.13 Schematics of Crack Propagation in Specimen 6-II-IV-1.

Figure 4.14 Schematics of Crack Propagation in Specimen 6-II-IV-2.
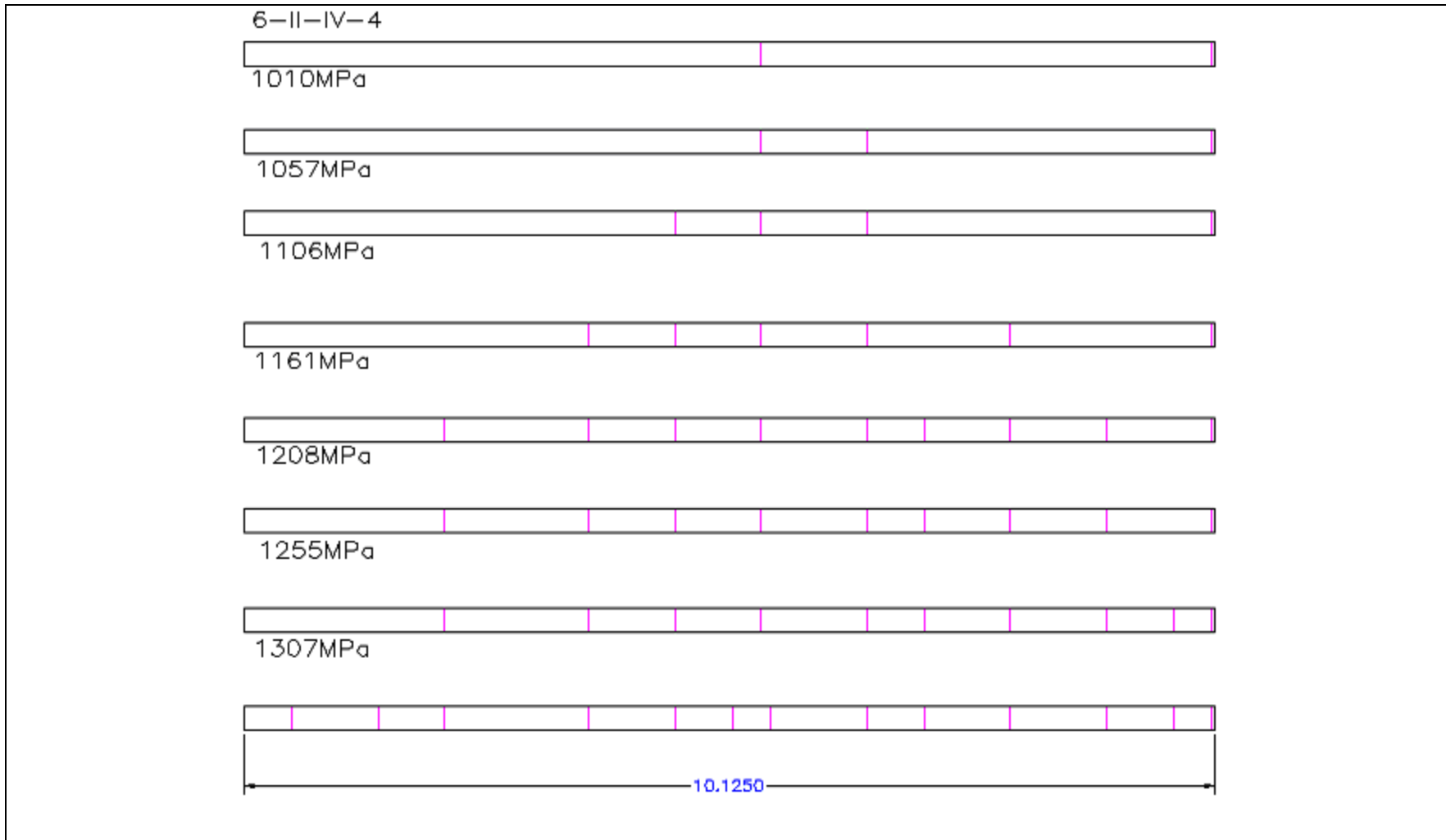
Figure 4.15 Schematics of Crack Propagation in Specimen 6-II-IV-4.
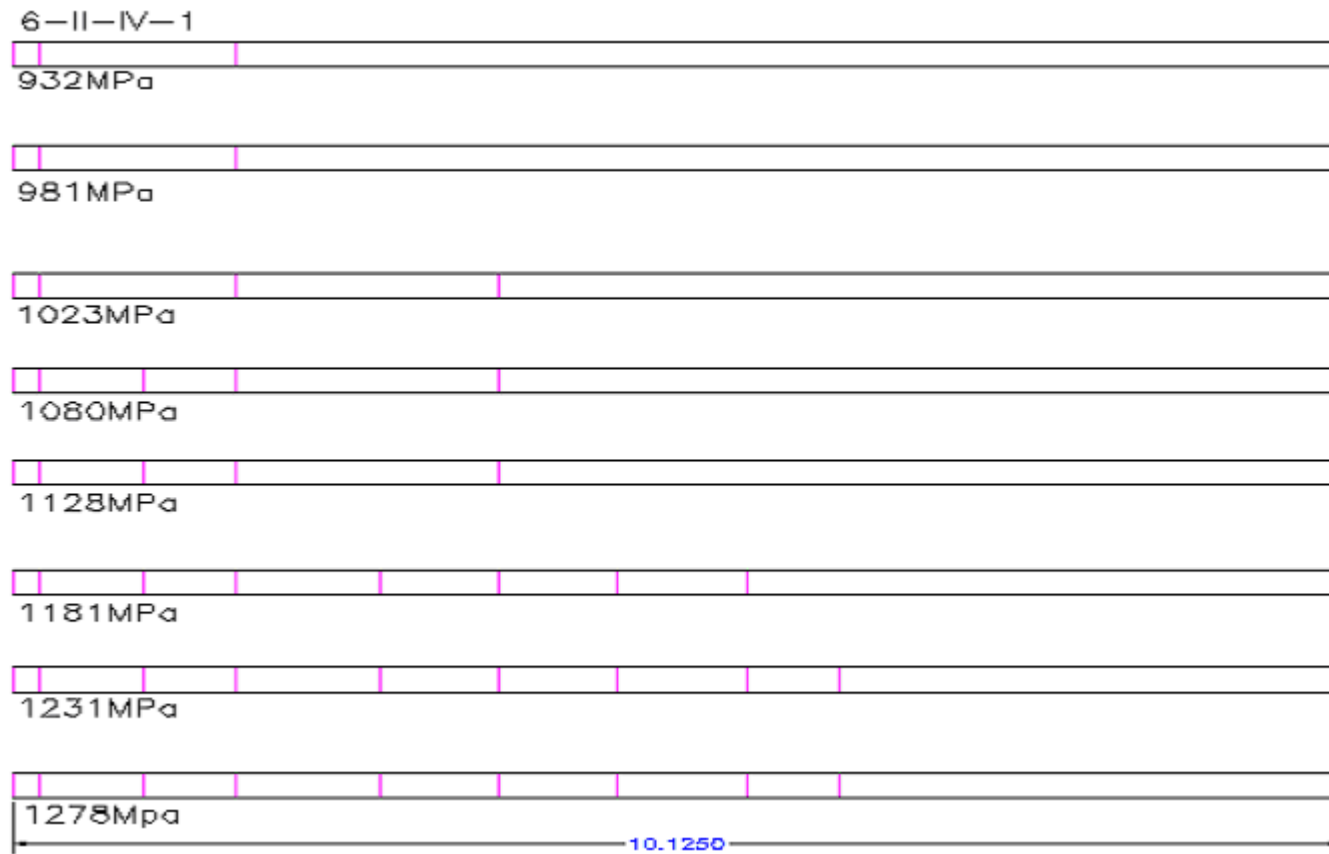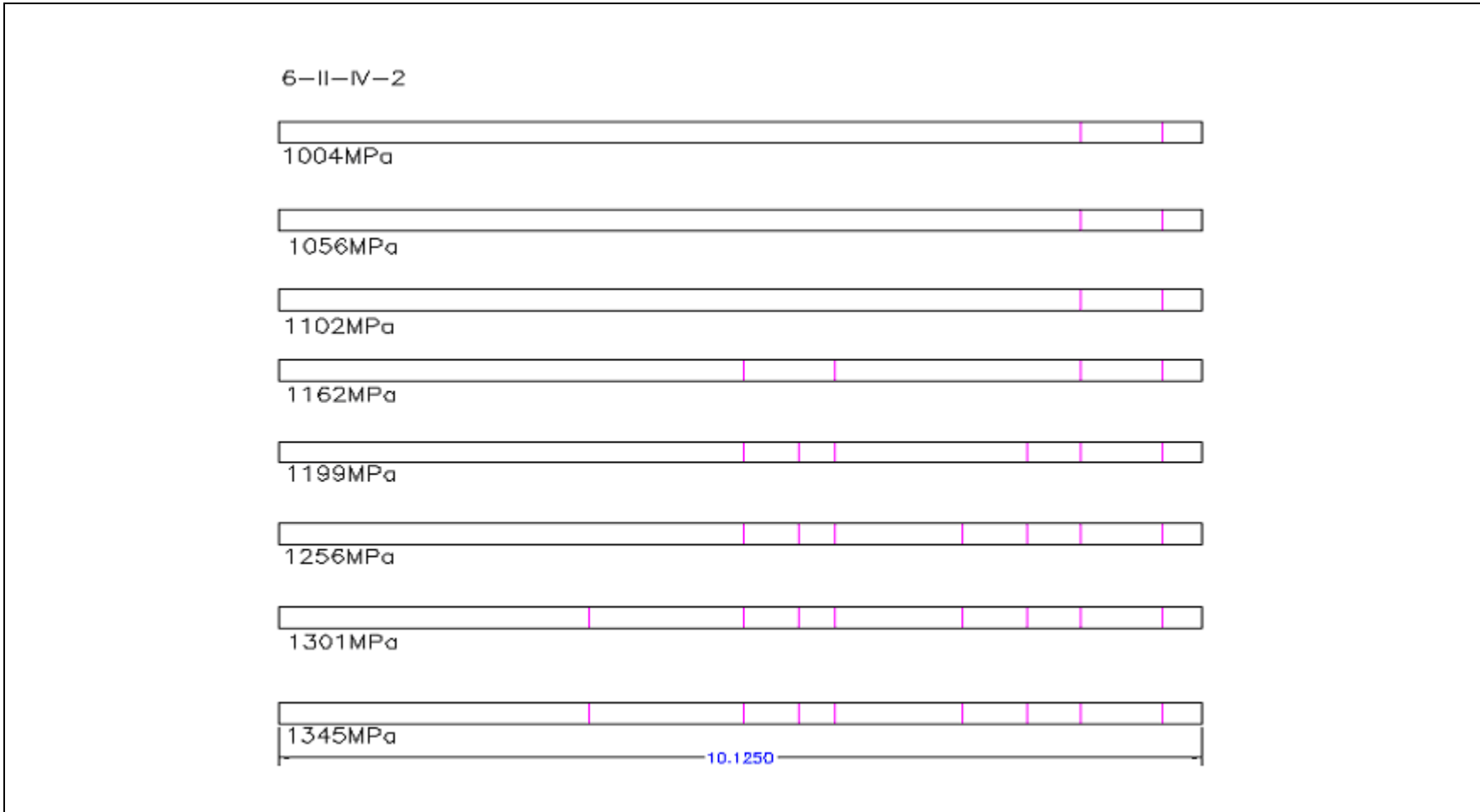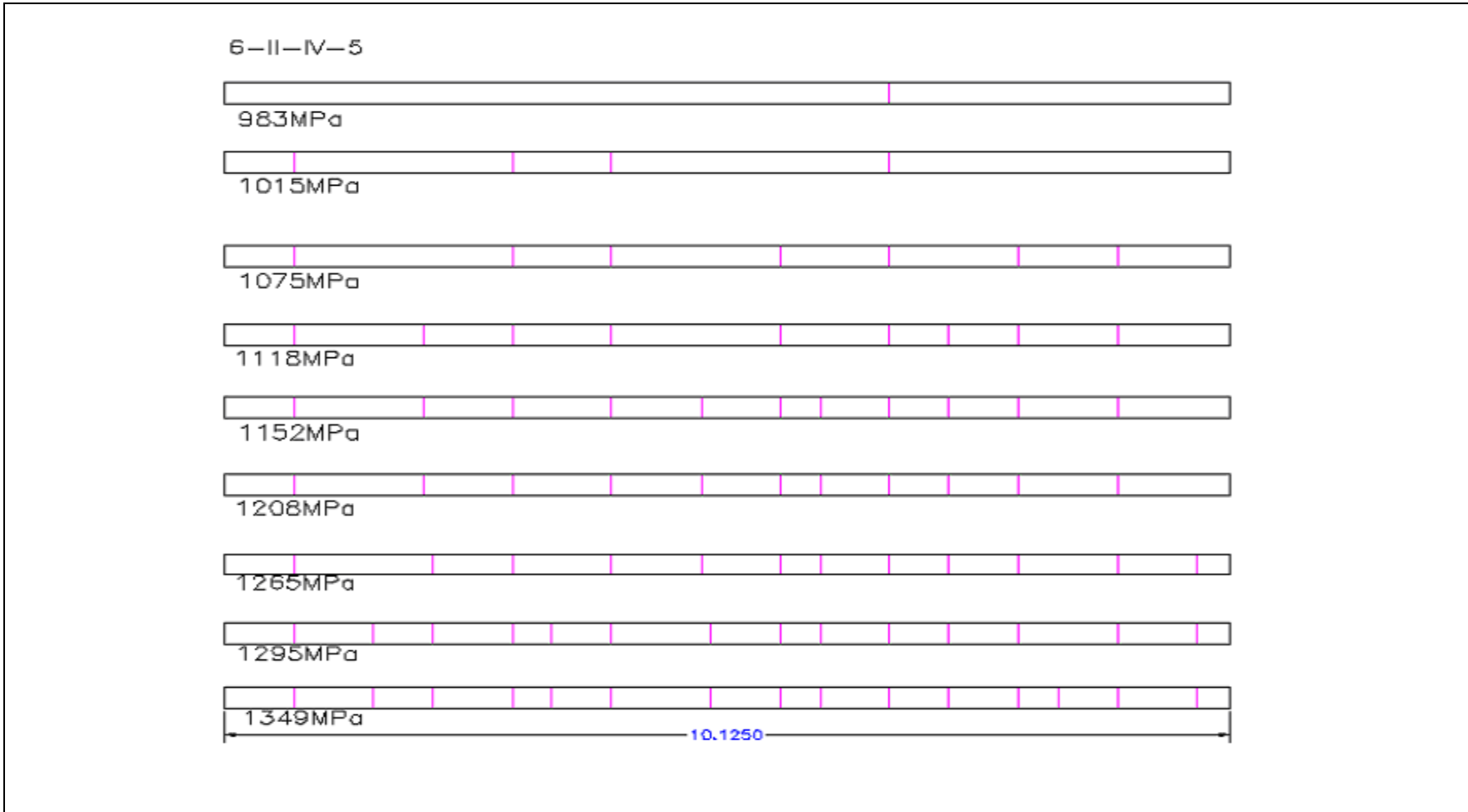
Figure 4.16 Schematics of Crack Propagation in Specimen 6-II-IV-5.
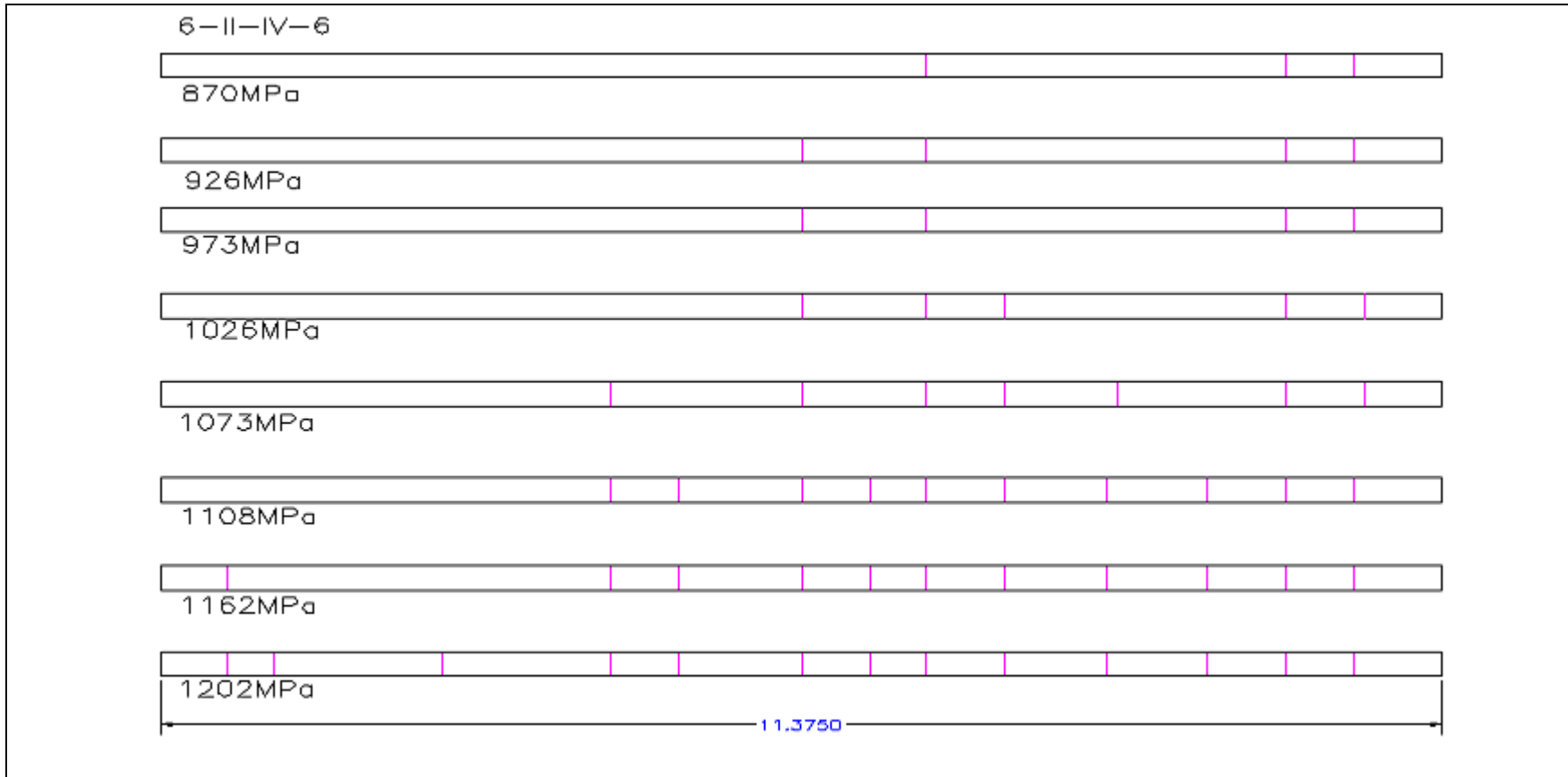
Figure 4.17 Schematics of Crack Propagation in Specimen 6-II-IV-6.
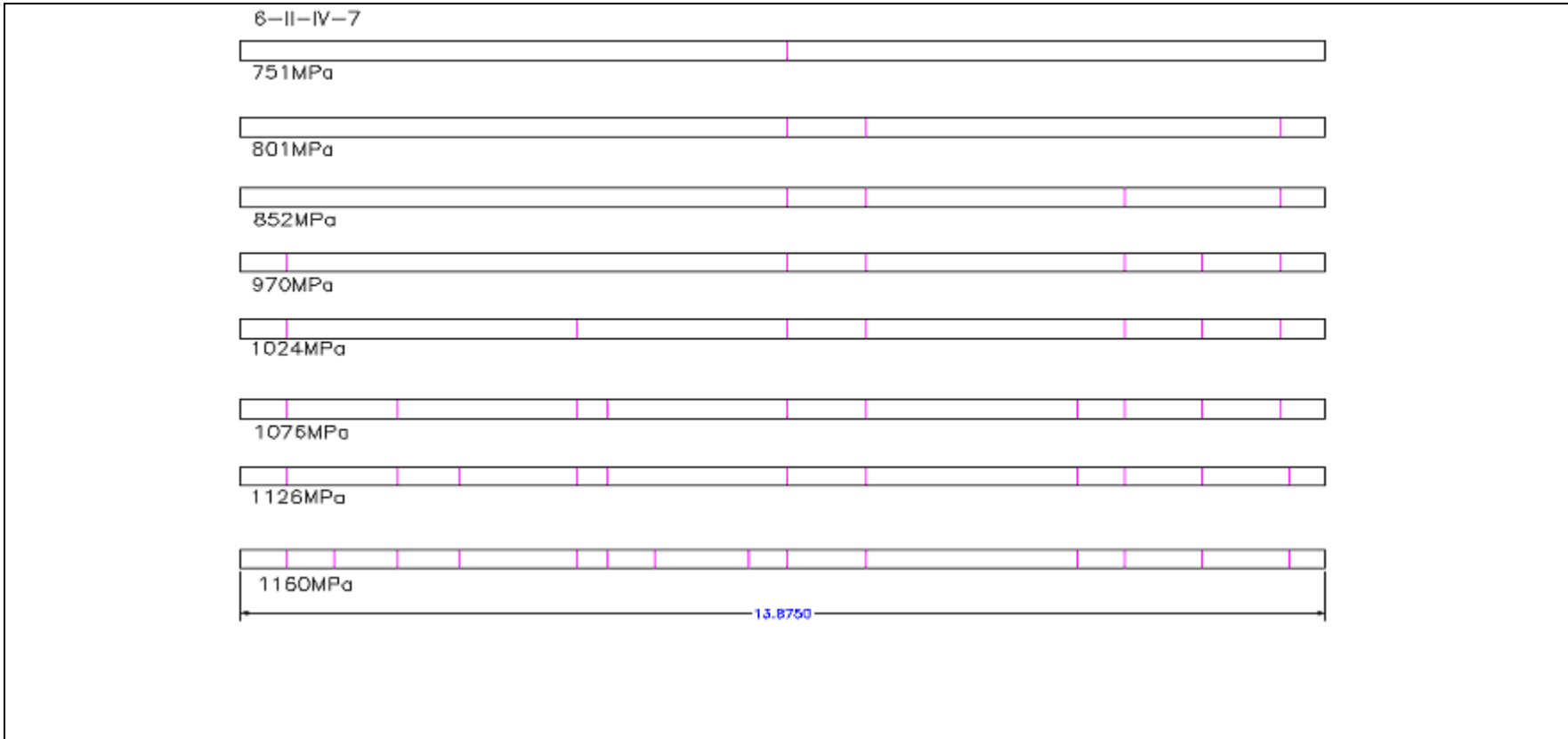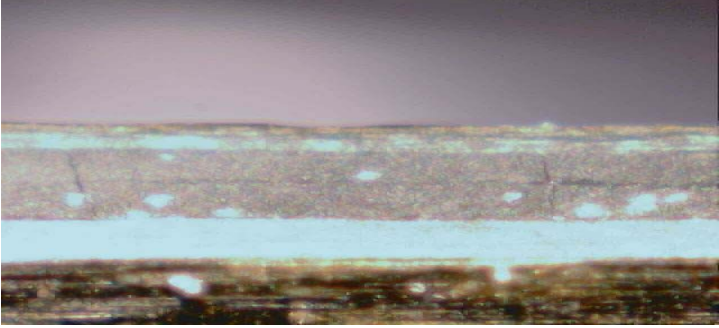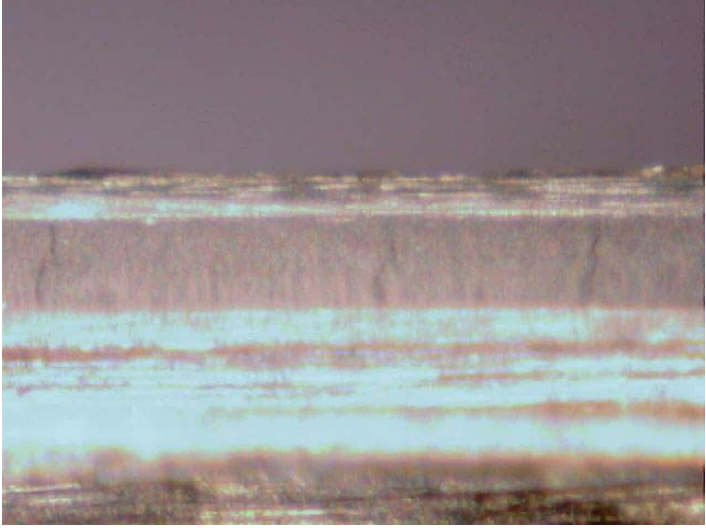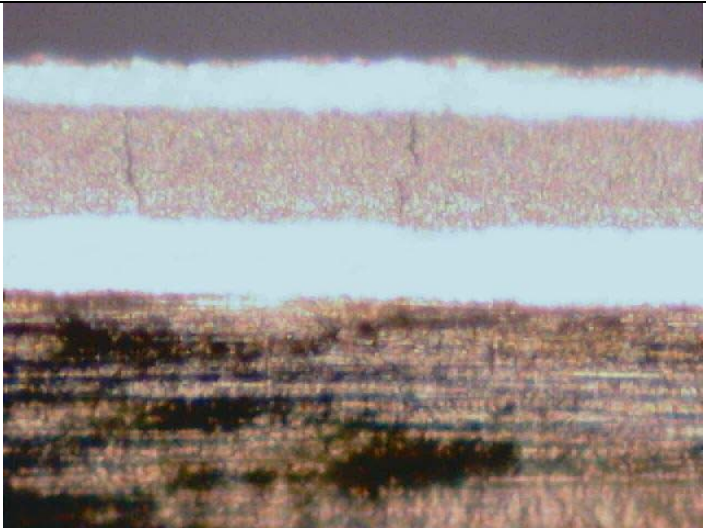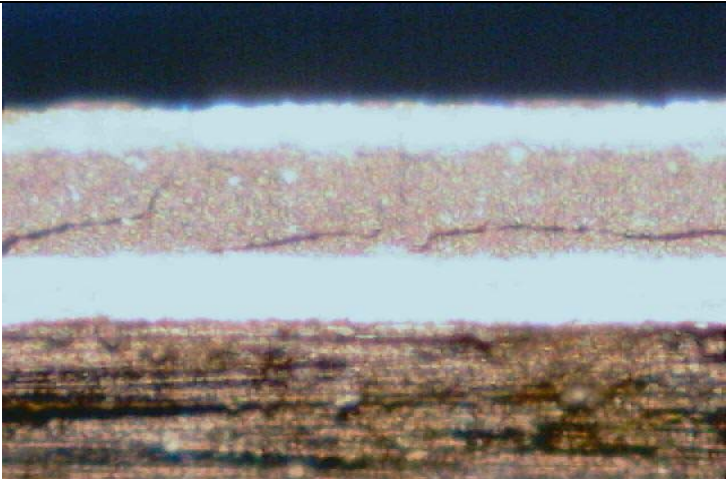
Figure 4.18 Schematics of Crack Propagation in Specimen 6-II-IV-7.
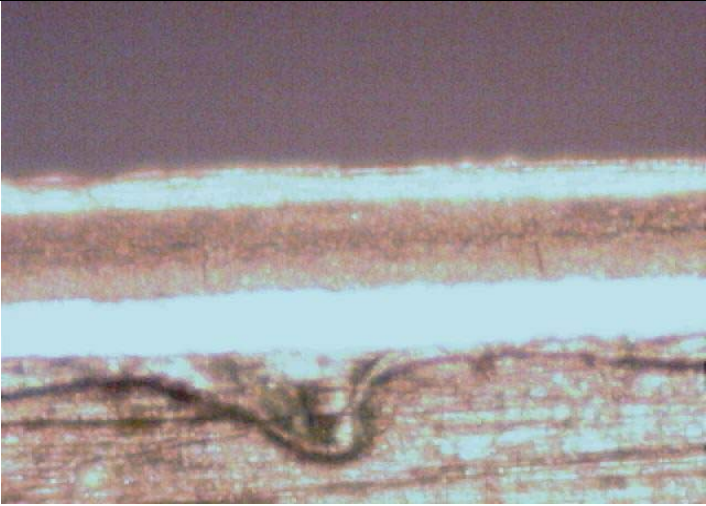
These specimens had different optical span lengths under investigation. Not all of the specimens started microcracking at the center of the specimen. The material system IM7/5276-1 showed very little damage in addition to microcracking under the optical microscope. Only two specimens started delaminating just before failure. The discussion of the damage is presented in Table 4.6.

Table 4.6 Micrograph Observations for Material System IM7/5276-1.

Specimen	Micrograph	Damage Load (MPa) and Discussions
6-II-IV-1		The micrograph in the left is from specimen 6-II-IV-1 at 1262MPa. The specimen did not show other forms of damage other than microcracks and failed near the tabs at 1262MPa.
6-II-IV-2		The micrograph in the left is from specimen 6-II-IV-2 at 1256MPa. The specimen did not show other forms of damage other than microcracks and failed into two pieces in the mid span at 1256MPa.

6-II-IV-4		The micrograph in the left is from specimen 6-II-IV-4 at 1358MPa. As seen in the micrograph, the specimen developed fiber pull-out in the 0° plies. The specimen failed at 1381MPa near the tabs.
6-II-IV-5		The micrograph in the left is from specimen 6-II-IV-5 at 1295MPa. The specimen did not show any damage other then microcracks and failed near the tabs at 1349MPa.

6-II-IV-6		The micrograph in the left is from specimen 6-II-IV-6 at 1202MPa. The specimen did not show any damage other then microcracks and failed near the tabs at 1202MPa.
6-II-IV-7		The micrograph in the left is from the specimen 6-II-I-7 at the load of 1160MPa. As seen in the micrograph, the specimen did not delaminate at this location and a longitudinal in the 90° was seen. This crack initiated at a location left of this micrograph and is shown in the next micrograph. The specimen failed immediately into two pieces at 1160MPa. At this location fiber pull-out is seen.

6-II-IV-3		The micrograph in the left is from specimen 6-II-IV-1 at 1310MPa. The specimen did not show any damage other than microcracks and failed under the tabs at 1357MPa.

4.4 Comparison of Failure Behavior

For some of the IM7/977-2 specimens delamination and fiber pull-out was seen. Most of the specimens failed either at the ends or broke into two pieces at the mid-span. Material system IM7/5276-1 showed similar behavior in terms of damage and failure. This material system did not develop delamination; other forms of damage were also less frequent under the optical microscope. Like material system IM7/977-2, the specimens failed near the tabs or in the mid-span into two pieces. For material system IM7/5555 fiber pull-out and delamination were predominant and most of the specimens failed at an additional load around 250MPa after delamination. The material system at failure shattered into pieces; this characteristic is unique to this material system.

4.5 Comparison of Microcrack Propagation

A plot of microcracking density and applied load was plotted for all the specimens from all three material systems. Figures 4.19, 4.20 and 4.21 display the plot of microcracking density (cracks/cm) and applied stress (MPa).

Stress v/s Microcracking Density (IM7/977-2)
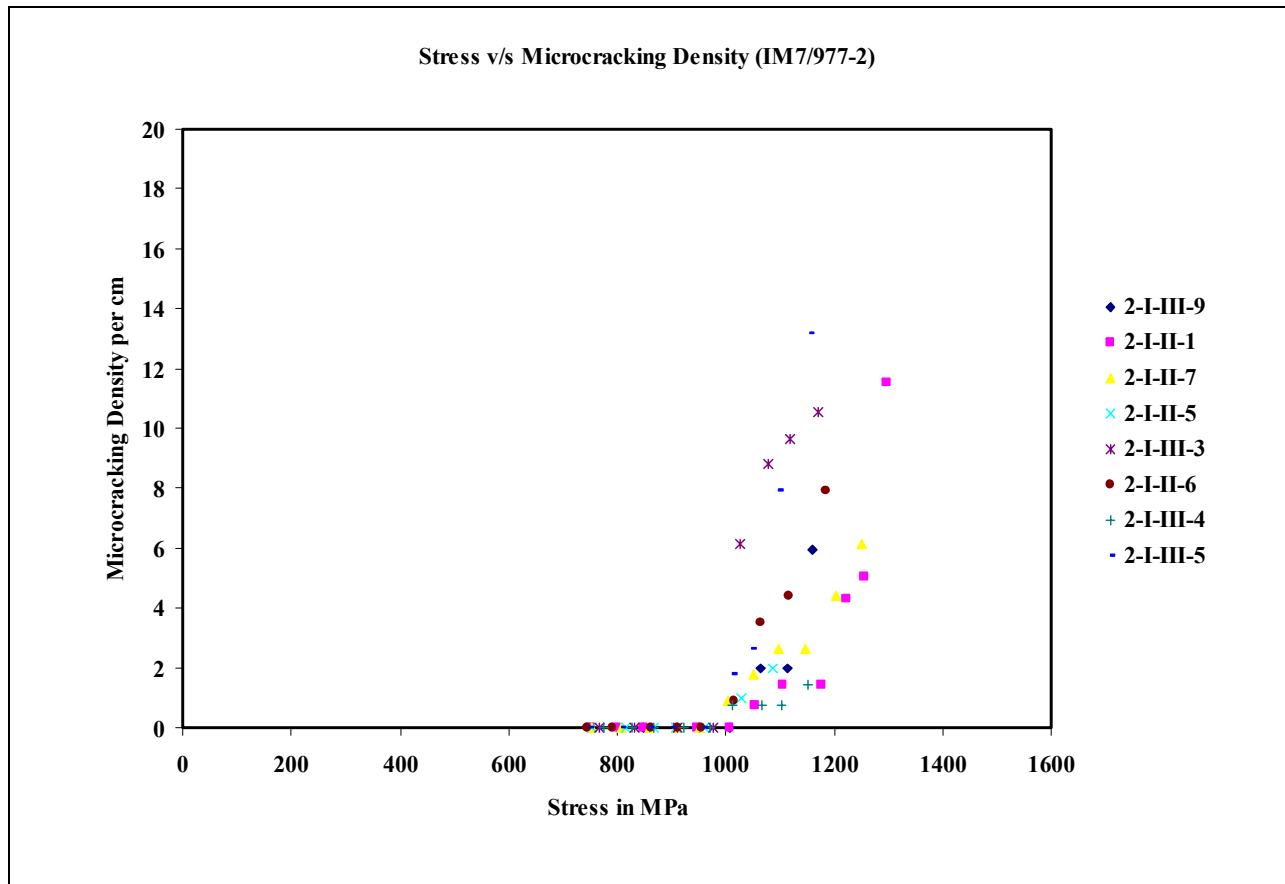
Figure 4.19 Plot of Microcracking Density versus Applied Stress for Material System IM7/977-2.

A plot of applied stress and microcracking density (in number of cracks per centimeter) for material system IM7/977-2 is shown in Figure 4.19. From the graph it can be seen that microcracks started to form at around 1000MPa to 1050MPa. After the onset of the first cracks the number of cracks increased immediately as the stress was increased. The maximum crack density was found in specimen 2-I-III-5 to be 13cracks/cm.

Figure 4.20 is the plot of microcracking density as a function of applied stress for material system IM7/977-2 from the preliminary studies [1]. It can be seen that the material system shows the steep increase in crack density after the initiation of microcracks.
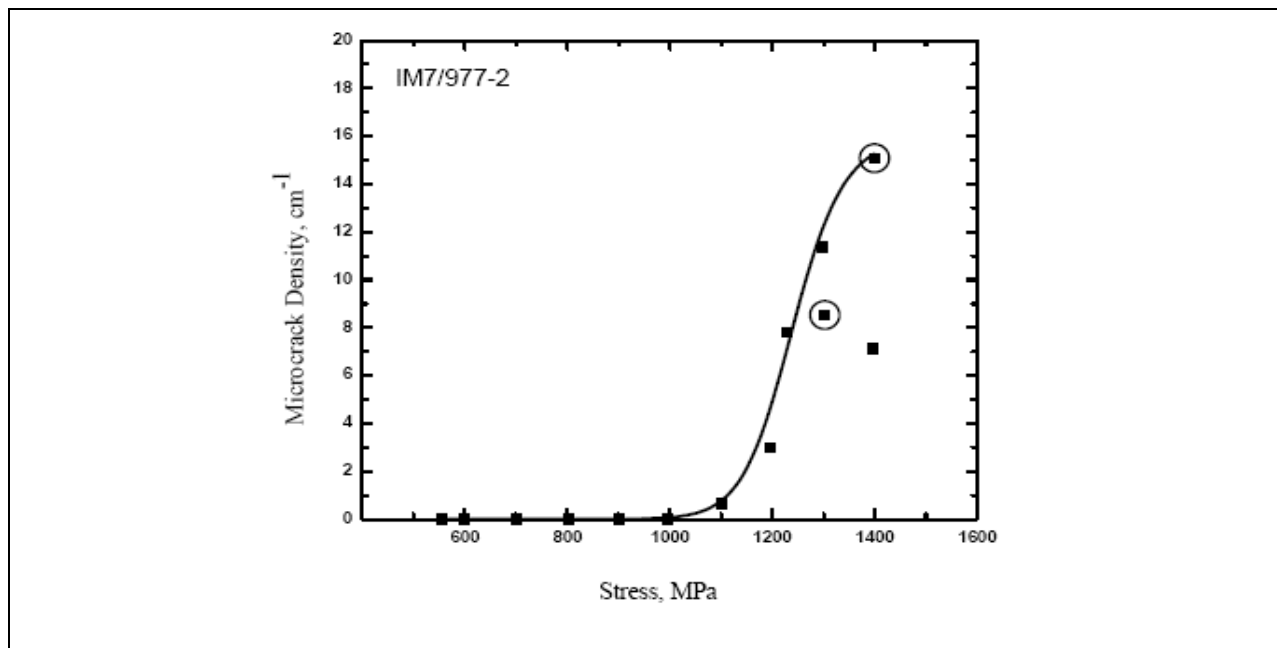
Figure 4.20 Plot of Microcracking Density versus Applied Stress for Material System IM7/977-2 from Ref [1].

From Figure 4.21 it can be seen that microcracks started forming in the range of 800MPa to 900MPa for material system IM7/5555. After the formation of the initial microcracks the increase in number of microcracks as a function of applied stress is not as steep as for material system IM7/977-2. The formation of microcracks is more gradual. Four of the six specimens tested to failure reached same crack density of 16.7cracks/cm before failure. Another observation is that the crack density remained the same for three of the specimens as the load was increased. From this, it can be concluded that the crack saturation density for the IM7/5555 material system is around 17cracks/cm.

Figure 4.21 Plot of Microcracking Density versus Applied Stress for Material System IM7/5555.

Figure 4.22 is the plot of microcracking density as a function of applied stress for material system IM7/5555 from the preliminary studies [1]. It can be seen that microcrack initiation in the preliminary studies occurred around 850MPa, but the when compared to the current results the increase in microcrack propagation appears to be steeper. This is because in the previous study the single specimen was not tested until failure and different specimens were loaded to a predetermined load; therefore each specimen's history was not analyzed. Because the current study is aimed at analyzing the microcracking history of each specimen and because more data points have been obtained, a clearer understanding of the microcracking trend has been attained.

In addition, the charts obtained in both the current study and the preliminary study both suggest that the material system reaches a crack saturation density of approximately 17 cracks/cm.
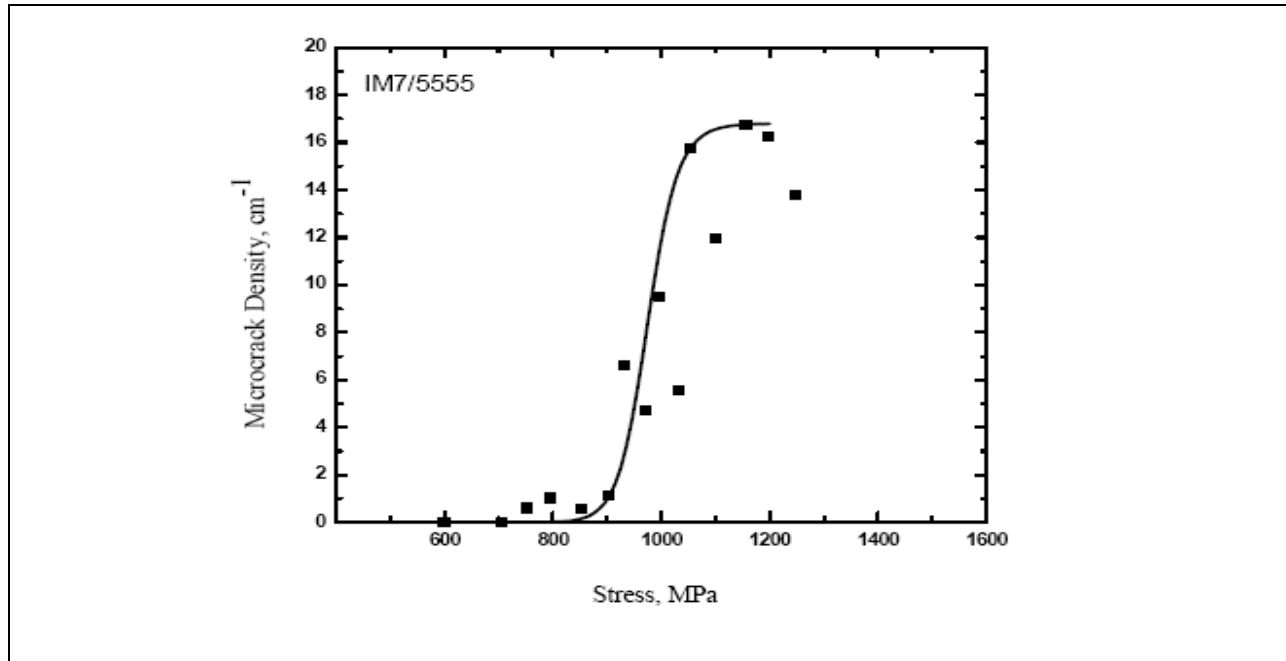
Figure 4.22 Plot of Microcracking Density versus Applied Stress for Material System IM7/5555 from Ref [1].

A plot of number of microcracks formed per centimeter as a function of applied stress is shown in the Figure 4.23 for material system IM7/5276-1. The starting stress for microcracking was more scattered and they started to microcrack between loads of 750 MPa and 950 MPa. There is no immediate increase in the number of microcracks after formation of the initial cracks and the slope of the function is not as steep as the slope of the IM7/977-2, and even the IM7/5555, data. It can also be noted that after the onset of microcracking the specimens failed at an additional average load of 340MPa, showing a dependence of initiation load to failure load. The average crack density for all seven specimens was around 11 cracks/cm. Specimen 6-II-IV-5 had the maximum number of microcracks with a microcracking density of 14.8cracks/cm.
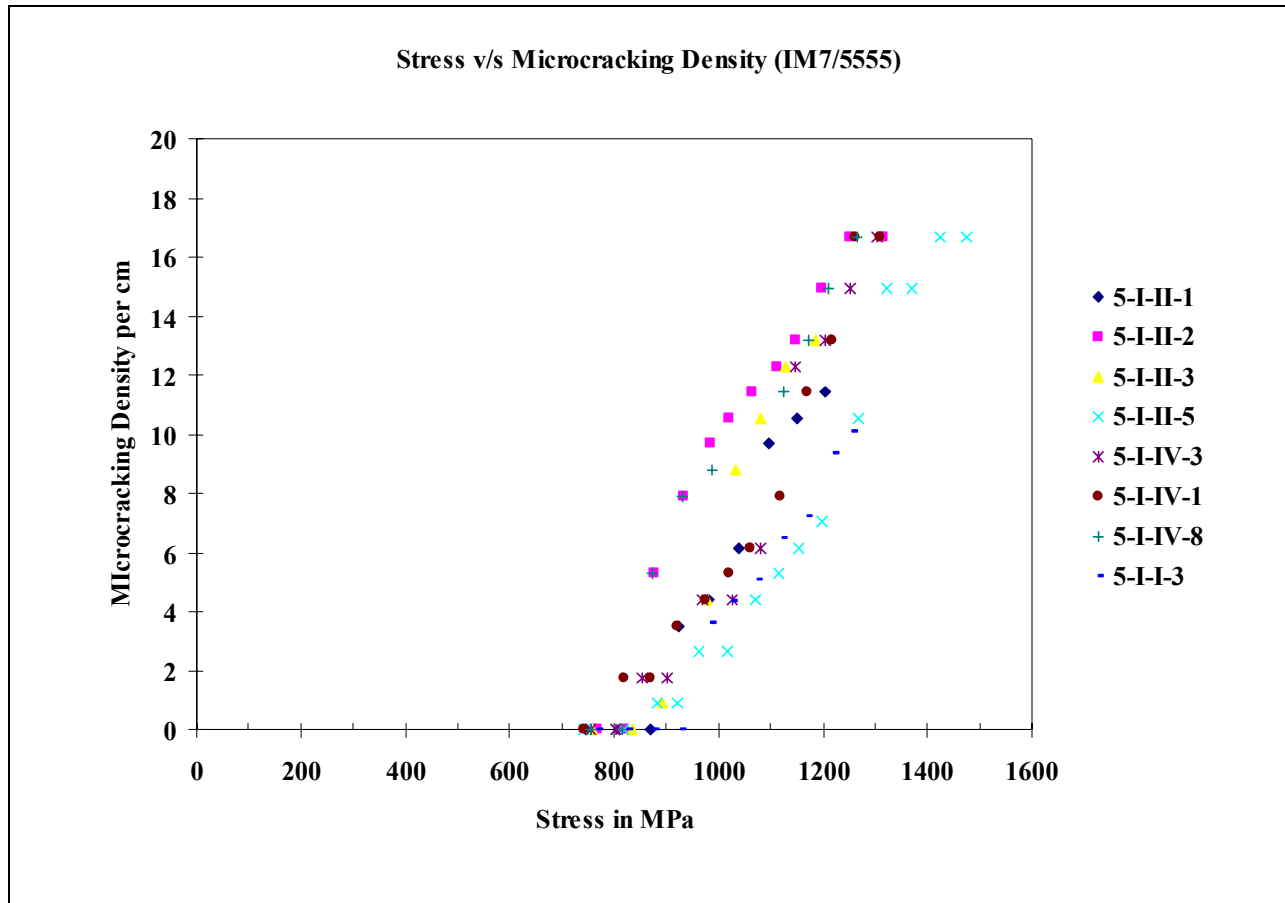
Stress v/s Microcracking Density (IM7/5276-1)
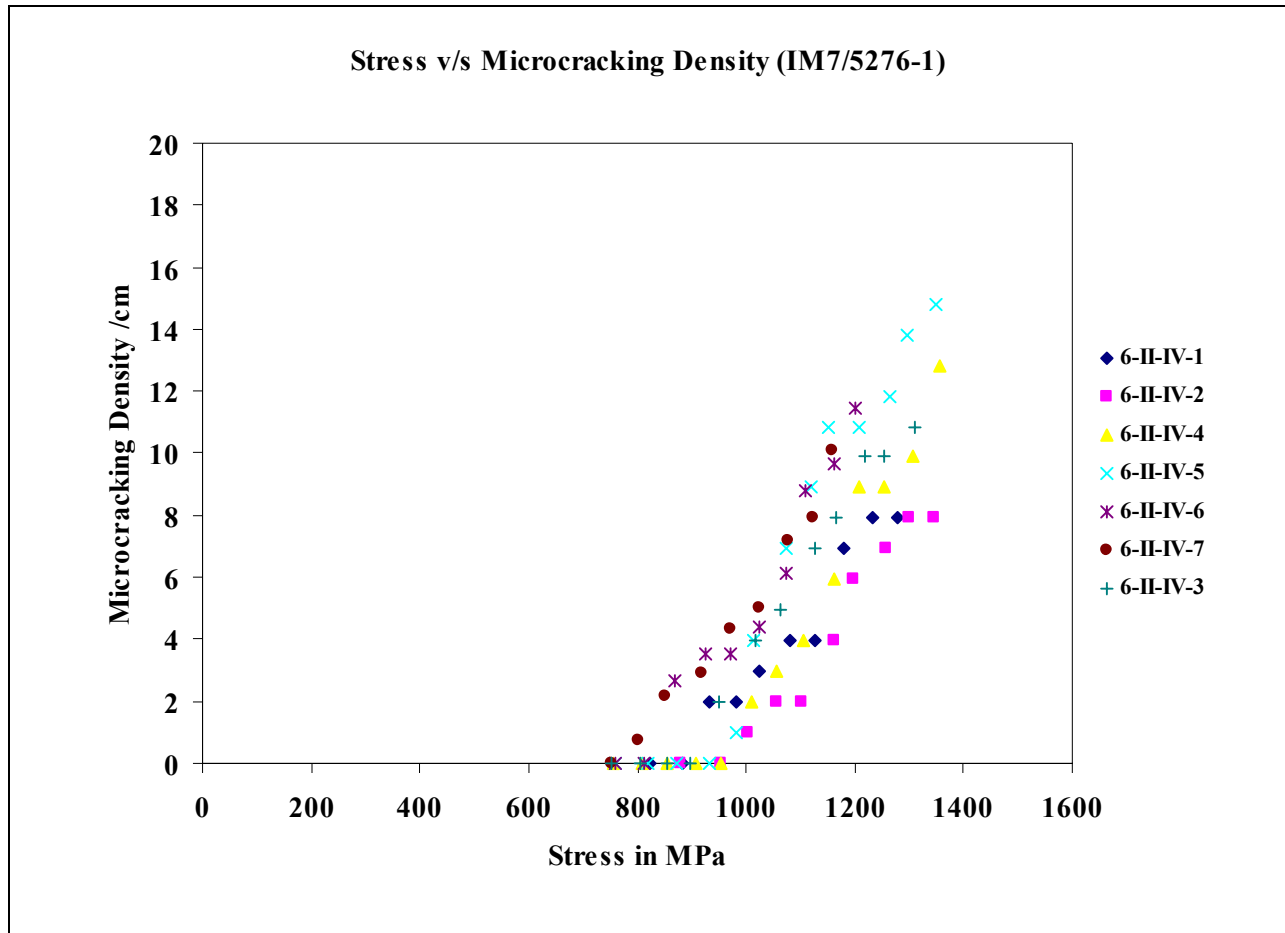
Figure 4.23 Plot of Microcracking Density versus Applied Stress for Material System IM7/5276-1.

Figure 4.24 a plot of microcracking density as a function of applied stress for material system IM7/5276-1 from the preliminary study [1]. From this plot it can be seen that microcrack initiation occurred around 850MPa. When comparing the microcracking density as a function of applied loading, the curve in the preliminary study is much steeper. However, again, in the preliminary study the history of each specimen was not analyzed and the number of data points was quite scarce. Also, the points with the circles in Figure 4.24 indicate that these samples failed. Note that they both failed at around 1100MPa. Of the specimens in the current study, the weakest one failed at 1160 MPa.
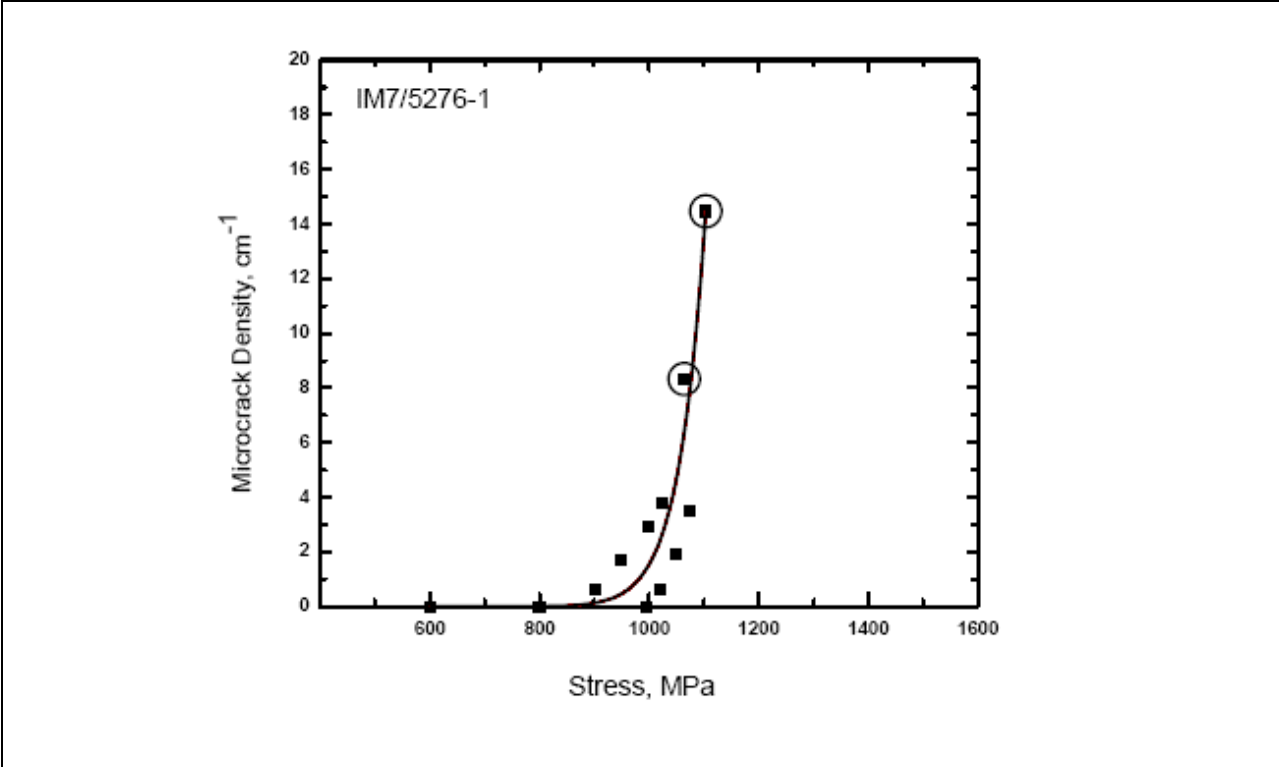
Figure 4.24 Plot of Microcracking Density versus Applied Stress for Material System IM7/5276-1 from Ref [1].

4.6 Microcracking Fracture Toughness for Material System IM7/977-2

As described in the literature review section, the microcracking fracture toughness, G_m, is useful in determining when microcracking will initiate and progress in a material system under a uniaxial loading. For material system IM7/977-2, the microcracking toughness is calculated using the material properties listed in Table 4.7.

Table 4.7 Input Material Properties for IM7/977-2.

Property	Value
E_a (Axial Modulus ply material)	159GPa
E_t (Transverse Modulus of ply material)	9.2GPa
E_c (x- direction modulus of cross-ply laminate)	84.2GPa
G_a (Axial Shear modulus)	4.37GPa
G_t (Transverse Shear modulus)	2.57GPa
α_a (Axial thermal expansion coefficient)	-0.09 ppm/^{o}C
α_t (Transverse thermal expansion coefficient)	28.8 ppm/^{o}C
v_a (Axial Poisson's Ratio)	0.253
v_t (Transverse Poisson's Ratio)	0.456
T_{eff} (Stress free temperature)	-125 ^{o}C

Of the above properties, E_a, E_c, E_t, G_a, G_t, v_a and v_t were provided by the manufacturer of the specimens, Lockheed Martin Corporation. The α_a and α_t values that were used are common for most material systems that are examined [11]. T_{eff}, the stress-free temperature, is basically the difference between the curing temperature (177°C) and room temperature (24°C). To account for the possibility of some relaxation at high temperatures T_{eff} is taken to be -125°C. The ply

thickness of 0.1375mm was also provided by the manufacturer. After accumulating these properties the only required inputs were the crack spacings, a, and the crack density, D, at each stress level. Using the equations that are described in Chapter 2 the value for the microcracking fracture toughness was found for material system IM7/977-2 using Microsoft Excel. The calculated microcracking fracture toughness for different values of f are displayed in the Table 4.8

Table 4.8 Microcracking Toughness for each Specimen at different f values.

Specimen	f=1.0	f=1.2	f=1.3	f=1.44
2-I-III-1	675.47	701.57	710.54	719.31
2-I-II-7	670.94	671.64	671.49	671.26
2-I-III-3	533.10	588.98	604.14	616.46
2-I-III-9	635.52	636.33	636.12	635.82
2-I-II-6	631.82	643.08	645.05	646.01
2-I-II-5	561.32	561.32	561.32	561.32
Average G_m	618.03	633.82	638.11	641.70

For each specimen at each stress level, the values of $\chi\ (\rho)$ at each crack spacing, a_i, (where i goes from I to n, with n being the total number of crack spacings) was calculated and the average vale of $\chi\ (\rho)$ was plotted as function of crack density. Therefore, each specimen has one data point corresponding to the average $\chi\ (\rho)$ value for each stress level. The results are depicted in Figure 4.25. In this plot the solid line represents the theoretical curve, i.e., the curve generated under the assumption that cracks will form in the mid-span of the existing cracks.

It can be observed from the graph that the χ (ρ) function is somewhat constant up to crack densities of 800 cracks per meter (8 cracks per centimeter) for the IM7/977-2 system. (Looking back to chapter 2 one can see that this χ (ρ) function is dependent only on the material properties of the system.) This region is typically called the low crack density regime. Note also from the graph that the most of the data points fall in the low crack density regime. Only two specimens displayed crack densities in the medium crack density regime, these specimens are 2-I-III-1 and 2-I-III-3. However, the data points corresponding to those specimens did not fall on the theoretical curve. It was also noted that these two specimens delaminated and failed immediately. Data points for specimen 2-I-III-3 are not represented in Figure 4.25 because of the low χ (ρ) value. It can be noted in Figure 4.25 the low χ (ρ) value of the data point in medium crack density regime for specimen 2-I-III-1. By observing Figure 4.5 it is also apparent that for specimen 2-I-III-9 the cracks formed in a small region. Therefore, the average crack spacing for this specimen at higher loads is quite higher than the corresponding crack densities. It can be concluded that the presence of the delamination caused the specimens to display a locally higher apparent crack density than the actual crack density. It should also be noted that for the same cross-ply laminate orientation, Nairn notes in one of his papers while studying T300/Fiberite 977-2 system that delamination occurred prior to being able to reach a high crack density regime [11].
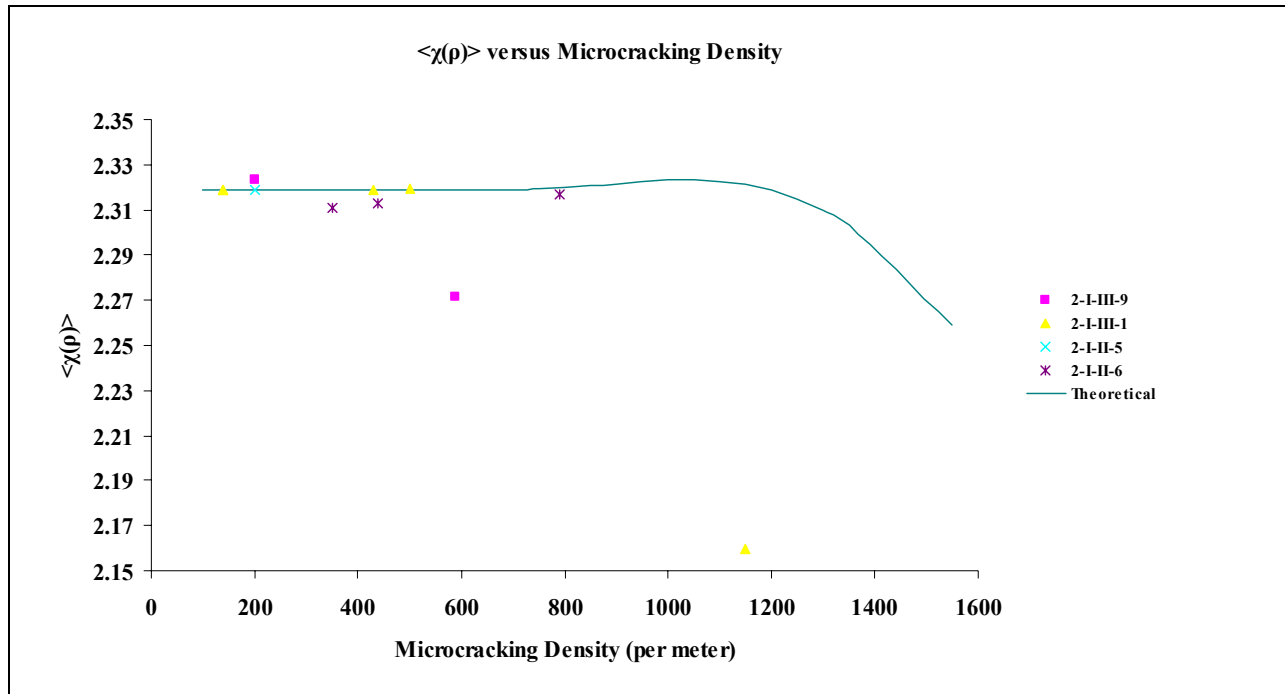
Figure 4.25 Plot of $<\chi(\rho)>$ as a function of Crack Density.

From Table 4.8 it can be noted that there is very little change in the values of microcracking fracture toughness with the change in the values of *f*. (Again, this is to be expected since *χ (ρ)* is constant in the low crack density regime.) There is a difference of only 4% in the calculated values when changing *f* from 1 to1.44. In the low crack density regime, it can be concluded that the microcracking fracture toughness is around $620J/m^2$.

5. Conclusions and Recommendations

The initiation and propagation of microcracks in IM7/977-2, IM7/5555 and IM/5276-1 cross-ply laminates were studied. From the plots of microcracking density versus applied stress it was observed the material system IM7/977-2 starts initiation of microcracking at higher loads than the other two systems. The IM7/977-2 material system also displays a steeper microcracking density versus applied loading curve than the other two systems. The material system IM7/5555 and IM/5276-1 showed microcracking initiation at lower loads and the increase in microcracking density is a gradual increase with respect to applied stress. The IM7/5555 is the only system that displayed saturation in the crack density (~17cracks per cm).

Of the three material systems, the IM7/977-2 system failed on the average at lower loads (~1220MPa). The other material systems failed on average around 1300MPa. While the IM7/977-2 and IM7/5276-1 system typically failed into two large pieces upon failure, the IM7/5555 specimens shattered into pieces. In addition, other types of damage, such as delamination and fiber pull-out, were observed in all of the material systems. However, it was noted that delamination occurred in a majority of the IM7/5555 specimens. These delaminations initiated at loads 250MPa lower than the failure load and microcracking densities around 10cracks/cm.

Compared to the initial studies, the microcracking density charts obtained in the current study display needed information. As observed from IM/5276-1 density charts, the additional data that

included the microcracking history of each specimen clarified that the initial steep trend shown in the preliminary study was not a true representation of the microcracking behavior.

The microcracking fracture toughness for IM7/977-2 was calculated to be around 620 J/m^2; the f parameter had minimal influence on the resulting toughness calculation (4% difference).

Increasing the optical span length to cover the gage length of the specimen would lend more information regarding the damage behavior. Also, inspecting the specimens at smaller load increments could potentially yield higher crack density information; this could be particularly useful in examining the f parameter for the IM7-977-2 specimens. Investigating other ply lay-ups for the IM7/977-2 material would give a better understanding of the microcracking behavior as well.

References

1. Melody A. Verges, Paul Schilling, Paul D. Herrington and Arun K. Tatiparthi, Investigation of Microcrack Growth in $[0/90]_S$ Composite Laminates, *ASME Pressure Vessels Piping Div Publ*, (2003) 171-175.

2. Bhagawan D. Agarwal and Lawrence J. Broutman, Analysis and performance of fiber composites.

3. J.A. Nairn and S. Hu, Micromechanics of Damage: A Case Study of Matrix Microcracking .Damage mechanics of composite materials, ed., Ramesh Talreja, Elsevier, Amsterdam (1994) 187-243.

4. John A. Nairn, Matrix Microcracking in Composites. Chapter 13 Polymer Matrix Composites.

5. K.W. Garrett and J.E. Bailey, Multiple Transverse Fracture in 90$^\text{o}$ Cross-Ply Laminates of Glass Fiber-Reinforced Polyester. *J. Mat. Sci* (1997) 157-168.

6. K.W. Garrett and J.E. Bailey, The Effect of Resin Failure on the Tensile Properties of Glass Fiber-Reinforced Cross-Ply Laminates. *J. Mat. Sci* (1997) 2189-2194.

7. J.A. Narin, S. Hu, S.Lui, and Bark, The Initiation, Propagation, and Effect of Matrix Microcracks in Cross-Ply Laminates. *Proc. Of the 1st NASA Advanced Composite Tech. Conf.*

8. J.A. Nairn, Microcracking, Microcrack-Induced Delamination, and Longitudinal splitting of Advanced Composite Structures. *NASA CR 4472* (1992).

9. J.A. Nairn and S. Hu, The Formation and Effects of Outer-Ply Microcracks in the Cross-Ply Laminates: A Variation Approach. *Eng. Fract. Mech*. 41 (1992) 203-221.

10. J. A. Nairn, S. Hu, and J.S. Bark, A Critical Evaluation of Theories for Predicting Microcracking in composite Laminates. *J. Mat. Sci.* 28 (1993) 5099-5111.

11. S. Lui and J.A. Nairn, The Formation and Propagation of Matrix Microcracking in Cross-Ply Laminates During Static Loading, *J. Reinf. Plast. and Comp.* 11 (1992) 158-178.

12. S. Hu, J.S. Bark, and J.A. Nairn, On the Phenomenon of Curved Microcracking in $[(S)/90_n]_s$ Laminates: Their Shapes, Initiation Angles, and Locations. *Comp. Sci. & Tech* 47 (1993) 321-329.

13. S.C. Tan and R.J. Nuismer, A Theory for Progressive Matrix Cracking in Composite Laminates, *J. Comp. Mat.* 23 1989 1029- 1047.

14. Norman Laws and George J. Dvorak, Progressive Transverse Cracking In Composite Laminates, J. Comp. Mat. 22 1988 900- 919.

15. J. A. Nairn, The Strain Energy Release Rate of Composite: A Variation Approach, *J. Comp. Mat.* 23 1989 1106-1129.

16. Cytec Engineering Materials CYCOM 977-2 Material Data Sheet.,1995.

17. Xiaofeng Su, Farnk Abdi and J. Andre Lavoie, Prediction f Micro-crack Densities in Cryogenic 1M7/977-2 Propellant Tanks 2004.

18. L. Boniface, S.L and Ogin, Application of the Paris Equation to the Fatigue Growth of Transverse Ply Cracks, *J. Comp. Mat.* 23 735-755.

19. Seth S. Kessler, Thad Matuszeski and Hugh McManus, The Effect of Cryocycling on the Mechnical Properties of IM7/977-2.

20. J.A. Nairn, Some New Variational Mechanics Results on Composite Microcracking, *Proceedings of ICCM-10* Canada.

Vita

Babruvahan Hottengada was born on April 15, 1981 in Mysore, India. He graduated with the Bachelors of Engineering degree in Mechanical Engineering form Vishweshwariah Technological University, India in 2002. He joined the graduate program in Mechanical Engineering at the University of New Orleans in 2003. Since then he has been working as a graduate research assistant under the guidance of Dr. Melody A Verges on BGA packing and Composite Material Matrix Microcracking. In May 2006 he earned his Masters in Science degree in Mechanical Engineering with his thesis entitled "Investigation of Microcrack Propagation and Damage Propagation in Cross-Ply Composite Laminates."